

University of Windsor

Scholarship at UWindor

Electronic Theses and Dissertations

Theses, Dissertations, and Major Papers

3-2-2021

QRS Complex Detection based on Multilevel Thresholding and Peak-to-Peak Interval Statistics

Sudipta Modak
University of Windsor

Follow this and additional works at: <https://scholar.uwindsor.ca/etd>

Recommended Citation

Modak, Sudipta, "QRS Complex Detection based on Multilevel Thresholding and Peak-to-Peak Interval Statistics" (2021). *Electronic Theses and Dissertations*. 8526.

<https://scholar.uwindsor.ca/etd/8526>

This online database contains the full-text of PhD dissertations and Masters' theses of University of Windsor students from 1954 forward. These documents are made available for personal study and research purposes only, in accordance with the Canadian Copyright Act and the Creative Commons license—CC BY-NC-ND (Attribution, Non-Commercial, No Derivative Works). Under this license, works must always be attributed to the copyright holder (original author), cannot be used for any commercial purposes, and may not be altered. Any other use would require the permission of the copyright holder. Students may inquire about withdrawing their dissertation and/or thesis from this database. For additional inquiries, please contact the repository administrator via email (scholarship@uwindsor.ca) or by telephone at 519-253-3000ext. 3208.

**QRS Complex Detection based on Multilevel Thresholding and
Peak-to-Peak Interval Statistics**

By

Sudipta Modak

A Thesis
Submitted to the Faculty of Graduate Studies
through the Department of Electrical and Computer Engineering
in Partial Fulfillment of the Requirements for
the Degree of Master of Applied Science
at the University of Windsor

Windsor, Ontario, Canada

©2020 Sudipta Modak

**QRS Complex Detection based on Multilevel Thresholding and
Peak-to-Peak Interval Statistics**

By

Sudipta Modak

APPROVED BY:

L. Rueda
School of Computer Science

N. C. Kar
Department of Electrical and Computer Engineering

E. Abdel-Raheem, Advisor
Department of Electrical and Computer Engineering

15th of December 2020

DECLARATION OF CO-AUTHORSHIP AND PREVIOUS PUBLICATION

I Co-Authorship

I hereby declare that this thesis incorporates material that is result of joint research, as follows:

The works showed in chapters 2, 3 and 4 were co-authored by me, Dr. Luay Yassin Taha and my supervisor Dr. Esam Abdel-Raheem. In all cases, the key ideas, experimental designs, data analysis, interpretation were conducted by the author and the writings were also carried out by the author.

I am aware of the University of Windsor Senate Policy on Authorship and I certify that I have properly acknowledged the contribution of other researchers to my thesis and have obtained written permission from the co-author(s) to include the material(s) in my thesis.

I certify that, with the above qualification, this thesis, and the research to which it refers, is the product of my own work.

II Previous Publication

This thesis includes 3 original articles that have been previously submitted for publication in peer reviewed journals and conferences, as follows:

Chapter	Publication Title	Publication Status
2	QRS Detection Using Multi-dimensional Thresholds and Statistical False Peak Elimination	Submitted for publication
3	Single Channel QRS Detection Using Discrete Wavelet Transform and Median Denoising With Adaptive Multilevel Thresholding.	Submitted for publication
4	QRS Detection Using Adaptive Multilevel Thresholding, Segmentation and Statistical False Peak Elimination	To be submitted for publication

I certify that I own the copyright for the above material(s) in my thesis that have been submitted for publication. I certify that the above material describes work completed during my registration as a graduate student at the University of Windsor.

III General

I declare that, to the best of my knowledge, my thesis does not infringe upon anyone's copyright nor violate any proprietary rights and that any ideas, techniques, quotations, or any other material from the work of other people included in my thesis, published or otherwise, are fully acknowledged in accordance with the standard referencing practices. Furthermore, to the extent that I have included copyrighted material that surpasses the bounds of fair dealing within the meaning of the Canada Copyright Act, I certify that I have obtained a written permission from the copyright owner(s) to include such material(s) in my thesis.

I declare that this is a true copy of my thesis, including any final revisions, as approved by my thesis committee and the Graduate Studies office and that this thesis has not been submitted for a higher degree to any other University or Institution.

ABSTRACT

Heart beats are important aspects of the study of heart diseases in medical science as they provide vital information on heart disorders and diseases or abnormalities in the heart rhythm. Each heart beat provides a QRS complex in the electrocardiogram (ECG) which is centered at the R-peak. The analysis of ECG is hindered by low-frequency noises, high-frequency noise, interference from P and T waves, and change in QRS morphology. Therefore, it is a major challenge to detect the QRS complexes using automatic detection algorithms.

This thesis aims to present three new peak detection algorithms based on a statistical analysis of the ECG signal. In the first algorithm, a novel method of segmentation and statistical false peak elimination is proposed. The second algorithm uses different levels of adaptive thresholds to detect true peaks while the third algorithm combines and modifies the two proposed algorithms to provide better efficiency and accuracy in QRS complex detection. The proposed algorithms are tested on the MIT-BIH arrhythmia and provides better detection accuracy in comparison to several state-of-the-art methods in the field. To evaluate the performance of the proposed method, the merits of evaluation consider the number of false positives and negatives. A false positive (*FP*) is the result of a noise peak being detected and a false negative (*FN*) occurs when a beat is not detected at all. The methods emphasize better detection algorithms that detect peaks efficiently and automatically without eliminating the high-frequency noise completely and hence reduces the overall computational time.

DEDICATION

To my parents, Swapan Kumar Modak and Mukta Rani Modak - My light in darkness.

ACKNOWLEDGEMENTS

First, I express my gratitude to the Department of Electrical Engineering of University of Windsor, for providing me with the opportunity to conduct research and pursue the Master's degree. My solemn gratitude to Dr. Esam Abdel-Raheem who has been my mentor and guided me throughout my duration of studies at the University of Windsor. While being my supervisor in this academic period, he has enriched and trained me with vast knowledge and competitive skills. I am very much grateful to my committee members, Dr. Narayan Kar and Dr. Luis Rueda for their guidance, continuous support and advice. I am also very grateful to Dr. Luay Yassin Taha for reviewing the work and for helping with the data acquisition of several databases used in the research.

TABLE OF CONTENTS

DECLARATION OF CO-AUTHORSHIP AND PREVIOUS PUBLICATION	iii
ABSTRACT	v
DEDICATION	vi
ACKNOWLEDGEMENTS	vii
LIST OF TABLES	xi
LIST OF FIGURES	xii
LIST OF ABBREVIATIONS	xvi
1 Introduction	1
1.1 ECG Signal	1
1.1.1 The heart and the cardiac conduction system	2
1.1.2 ECG signal procurement	4
1.1.3 Irregularities in the ECG signal	5
1.1.4 Artifacts in ECG signal	7
1.2 QRS Complex and Ectopic Beat Detection	9
1.2.1 Problems with automatic QRS detection	9
1.2.2 Background of automatic peak detection in ECG signals	10
1.2.3 Motivation	16

1.3	Thesis Contribution	17
1.4	Thesis Objective and Outline	18
2	A Novel Method of QRS Detection Using Multidimensional Thresholds and Statistical False Peak Elimination	20
2.1	Introduction	20
2.2	Data Acquisition	21
2.3	The Proposed Method	21
2.3.1	Preprocessing	23
2.3.2	Peak detection using statistical peak-to-peak interval analysis	24
2.3.3	Post-processing	28
2.4	Experiment and Results	32
2.5	Comparison with the State-of-the-Art Methods	38
2.6	Conclusion	46
3	Single Channel QRS Detection Using Discrete Wavelet Transform And Median Denoising With Adaptive Multilevel Thresholding	47
3.1	Introduction	47
3.2	The Proposed Method	48
3.2.1	Preprocessing	48
3.2.2	Peak detection using adaptive multilevel thresholding	51
3.2.3	Post-processing	54
3.3	Experiment and Results	54
3.4	Conclusion	57
4	QRS Detection Using Adaptive Multilevel Thresholding, Segmentation and Statistical False Peak Elimination	60
4.1	Introduction	60
4.2	The Proposed Method	61
4.2.1	Preprocessing	61

4.2.2	Peak detection using adaptive multilevel thresholding and statistical peak-to-peak interval analysis	63
4.2.3	Post-processing	68
4.3	Experiment and Results	70
4.4	Conclusion	77
5	Conclusions and Future Work	78
5.1	Conclusions	78
5.2	Future Work	79
	BIBLIOGRAPHY	80
	VITA AUCTORIS	86

LIST OF TABLES

2.1	Vector classification	30
2.2	Results from the MIT-BIH arrhythmia database.	33
2.3	Results from Fantasia database	35
2.4	Comparison with state-of-the-art methods	38
2.5	Comparison of noisy records with three state-of-the-art methods	44
2.6	Comparison with T. Sharma et al. [13] on two databases	45
3.1	Results from the MIT-BIH arrhythmia database	55
3.2	Comparison with state-of-the-art methods	57
4.1	Results from the MIT-BIH arrhythmia database	71
4.2	Comparison with state-of-the-art methods	73
4.3	Comparison with methods in the developing stages	75

LIST OF FIGURES

1.1	ECG and QRS complex [1].	2
1.2	The heart [1].	3
1.3	The cardiac conduction system [4].	3
1.4	The Einthoven triangle formed by limb electrodes and the six leads [1].	5
1.5	The placement of leads on the chest [1].	6
1.6	ECG contaminated with powerline interference.	8
1.7	ECG contaminated with motion artifacts.	8
1.8	ECG contaminated with baseline wander.	9
1.9	ECG contaminated with EMG signal.	10
2.1	Block diagram of the proposed method.	22
2.2	Outputs obtained from different stages with y-axis in mV. (a) ECG signal from record 228 of MIT-BIH database, (b) Signal obtained after median filtering, (c) Signal obtained after preprocessing.	23
2.3	Outputs obtained from different stages with y-axis in mV. (a) ECG signal from record 228 of MIT-BIH database, (b) Peaks detected on the preprocessed signal, (c) Peaks detected on the original signal. The circles provided show the detected peaks on the corresponding signals.	25
2.4	False peaks between true positives.	28
2.5	False peak elimination in record 104 with y-axis in mV (277-347s) of MIT-BIH arrhythmia database. (a) False peaks detected after preprocessing, (b) False peaks eliminated after assessment.	29

2.6	Search back in record 109 with y-axis in mV (1039-1108s) of MIT-BIH arrhythmia database. (a) Peaks detected after False peak elimination, (b) Low amplitude peaks detected resulting from search back.	32
2.7	Outputs obtained from record 108 with y-axis in mV (222-236s). (a) Peak detected on preprocessed signal, where the pink circles provided show the detected peaks on $x_3(k)$. (b) Peaks detected on the baseline corrected signal where the red circles show the detected peaks on $x_2(k)$. (c) Peaks detected on the original signal where the red circles show the locations of the peaks in $x(k)$.	39
2.8	Outputs obtained from record 114 with y-axis in mV (291-305s). (a) Peak detected on preprocessed signal, where the pink circles provided show the detected peaks on $x_3(k)$, (b) Peaks detected on the baseline corrected signal where the red circles show the detected peaks on $x_2(k)$, (c) Peaks detected on the original signal where the red circles show the locations of the peaks in $x(k)$.	40
2.9	Outputs obtained from record 104 with y-axis in mV (56-70s). (a) Peak detected on preprocessed signal, where the pink circles provided show the detected peaks on $x_3(k)$, (b) Peaks detected on the baseline corrected signal where the red circles show the detected peaks on $x_2(k)$, (c) Peaks detected on the original signal where the red circles show the locations of the peaks in $x(k)$.	41
2.10	Outputs obtained from record 203 with y-axis in mV (0-14s). (a) Peak detected on preprocessed signal, where the pink circles provided show the detected peaks on $x_3(k)$, (b) Peaks detected on the baseline corrected signal where the red circles show the detected peaks on $x_2(k)$, (c) Peaks detected on the original signal where the red circles show the locations of the peaks in $x(k)$.	42
3.1	Block diagram for the proposed method.	48

3.2	Wavelet decomposition to three levels.	49
3.3	Wavelet transformed signals for scale level (1-3) for a section record 104 from the MIT-BIH arrhythmia database. (a) Raw ECG signal, (b) Detail signal for level 1, (c) Detail signal for level 2, (d) Detail signal for level 3, (e) Approximate signal for level 3.	50
3.4	Outputs obtained from different stages with y-axis in mV. (a) ECG signal from record 111 of MIT-BIH database, (b) Signal obtained after median filtering, (c) Envelope obtained after smoothing.	51
3.5	A section of record 108 from MIT-BIH arrhythmia database with y-axis in mV (388-416s). (a) Raw ECG signal, (b) Signal obtained after median filtering, (c) Peaks detected on the envelope of the signal. The green, red and black lines represent the non-adaptive threshold S , the upper adaptive threshold M and lower adaptive threshold R , respectively.	59
4.1	Block diagram of the proposed method.	61
4.2	Baseline wander removal. (a) ECG signal with baseline wander, (b) Bandpass filtered signal after removing baseline wander.	62
4.3	Powerline interference removal. (a) ECG signal with powerline interference, (b) Powerline interference removed after bandpass filtering.	63
4.4	Outputs obtained from record 104 with y-axis in mV (333-346s). (a) The raw ECG Signal, (b) The bandpass filtered signal, (c) The preprocessed signal.	64
4.5	Multilevel adaptive thresholding.	66
4.6	False peak elimination in record 104 with y-axis in mV (277-347s) of MIT-BIH arrhythmia database. (a) False peaks detected after pre-processing, (b) False peaks removed after using statistical false peak elimination.	69

4.7	False peak elimination in record 109 with y-axis in mV (222-236s) of MIT-BIH arrhythmia database. (a) False peak eliminated signal, (b) Missed peak detected on the preprocessed signal after using search back.	71
4.8	Peak detection performed in record 113 with y-axis in mV (125-139s). (a) The raw ECG signal, (b) Peaks detected on the ECG signal, (c) Peaks detected on the preprocessed signal.	76

LIST OF ABBREVIATIONS

AF - Atrial fibrillation

AMT- Adaptive multilevel thresholding

AV - Atrioventricular

aVF - Augmented voltage left foot

aVL - Augmented voltage left

aVR - Augmented voltage right

BPM - Beats per minute

coif - Coiflet

CWT - Continuous wavelet transform

Db - Daubechies

DER - Detection error rate

DLT - Down limited thresholds

DWT - Discrete wavelet transform

ECG - Electrocardiogram

EMG - Electromyogram

FIR - Finite impulse response

FN - False negative

FP - False positive

HHT - Hilbert Huang transform

IMF - Intrinsic mode function

LMS - Least mean squares

MA - Moving average MSE - Mean squared error

MTP - Missed true positives

P+ - Positive predicivity

PAC - Premature atrial contraction

PJC - Premature junctional complex

PVC - Premature ventricular contraction

RLS - Recursive least squares

SA - Sinoatrial

Se - Sensitivity

SNR - Sound to noise ratio

ULT- Up Limited thresholds

Chapter 1

Introduction

The human heart is the most important organ of the human body. It pumps oxygenated blood to all parts of the body, feeding cells with oxygen to produce their own energy. Any flaw in the heart is a threat to the human health and, therefore, monitoring its state is of the utmost importance in modern science. Electrocardiogram (ECG) is a non-invasive test of the heart that surveys the operability of the heart. It is a simple test, and it provides vital details of the heart's condition for cardiac patients. An ECG signal from an individual can reveal any anomalies associated with the heart's function and by studying the shapes and position of the heartbeats a proper diagnosis of heart associated diseases can be obtained.

1.1 ECG Signal

Electrocardiogram (ECG) is a recording of the action potential of the SA and AV nodes and the depolarizing cells of the heart [1]. The ECG signal can be detected using electrodes on the surface of the chest, arms and legs [2]. An ECG signal contains P waves, QRS complexes, and T waves. Figure 1.1 shows an ECG signal with its unique waveform. The P wave here is the result of the SA node depolarizing. It is a blunt, low amplitude wave that lasts for approximately 60 to 80 ms [1]. The QRS complex is triggered by the AV node. The Q wave is the result of depolarization of the interventricular septum, the R wave occurs when the main mass of the ventricles depolarize and the S wave represents the depolarization of the remainder of the wall cells of the ventricles [1]. The T wave occurs when the ventricular muscles repolarize and takes about 120 to 160 ms to complete [1]. Figure 1.1 shows the QRS complex

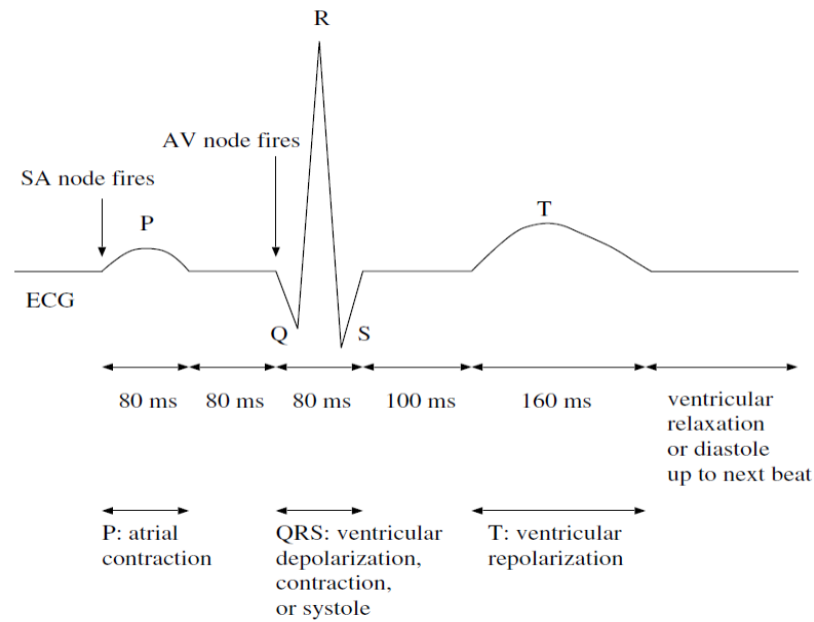


Figure 1.1: ECG and QRS complex [1].

with P and T waves. By studying the structure and intervals of these waves much information about the position, the chamber sizes, and the rhythm of the heart can be obtained.

1.1.1 The heart and the cardiac conduction system

The heart is a cone-shaped muscular pump [3] that resides in the chest cavity surrounded by the lungs and shielded by the breastbone and rib cage. It consists of four chambers, the right atrium, right ventricle, left atrium, and left ventricle. Figure 1.2 shows the cross-section of the heart with its chambers and vessels. The vena cava transfers blood to the right atrium which in turn pumps the deoxygenated blood to the right ventricle. The walls of the right ventricle are thinner compared to the left ventricle, as it pumps the blood to the lungs via pulmonary arteries. The left atrium receives the oxygenated blood from the lungs through the pulmonary veins and then pushes the blood into the left ventricle. The walls of the left ventricle are thick and well adapted for pumping the blood throughout the body via the aorta. This entire process can be performed several times every second to nourish the bodily tissues with a much-needed supply of oxygen.

A typical heartbeat starts with the initiation of the action potential in the sinoatrial (SA) node [2]. Figure 1.3 shows the pathway of the cardiac conduction system. The

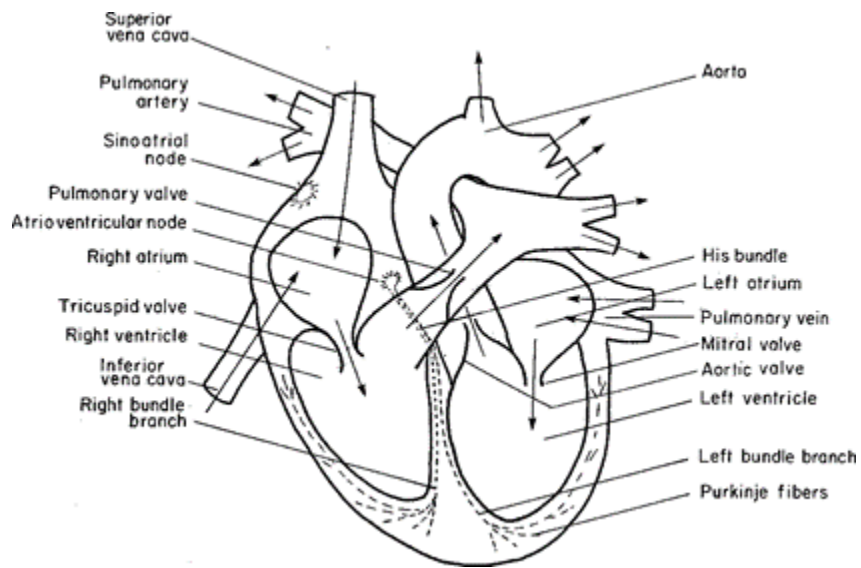


Figure 1.2: The heart [1].

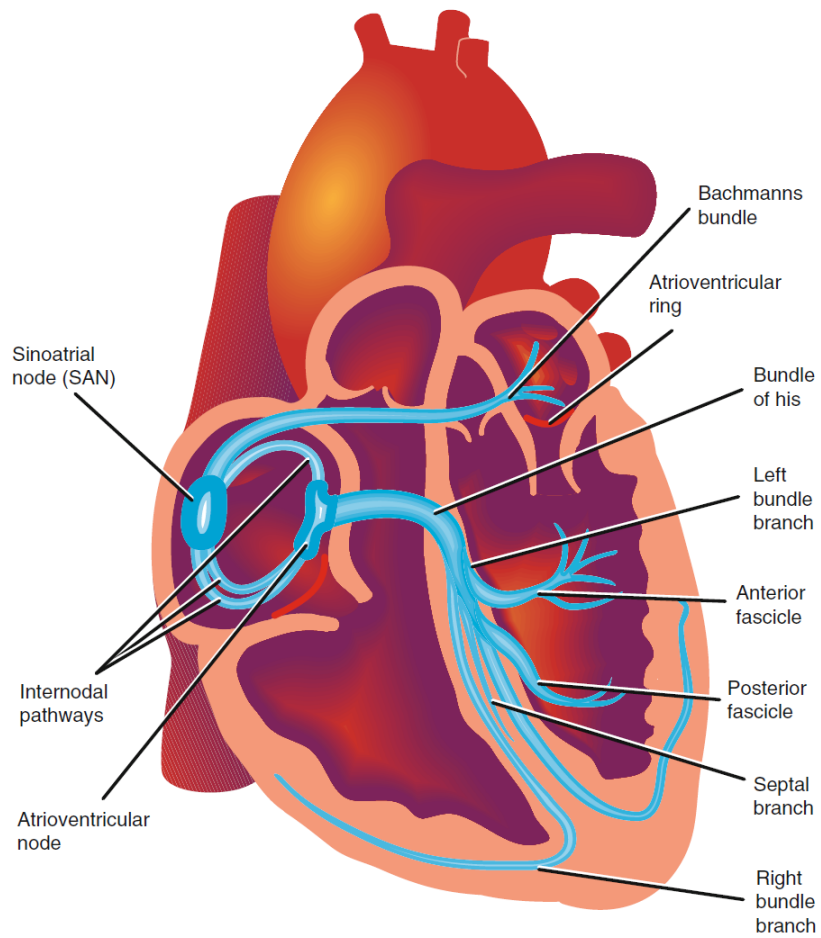


Figure 1.3: The cardiac conduction system [4].

SA node is the natural pacemaker of the heart and it depolarizes starting the cycle of heartbeat. The signal is passed throughout both atria using the internodal pathways and Bachmann's bundle and slowly lets the cells in the atria to depolarize. The signal is also picked up by the Atrio-ventricular node which delays the signal approximately 100 ms to ensure all cells of the atria have depolarized before passing the signal through the bundle of His to the walls of the ventricles. The atria and the ventricles are isolated from each other by a ring of fibrous tissue [2] which insulates the ventricular muscles from the atrial muscles. This is to prevent the atria and the ventricles from depolarizing at the same time. This ensures that the ventricles are filled up with blood and the atria are empty before the ventricles pump the blood. The AV node is the only link in terms of conductivity between the two regions. Once, the AV node has delayed the signal enough for the ventricles to be full, the signal is carried through the bundle of His. The bundle carries the signal first towards the apex and splits into two, the right and left bundle branches. The signal is then transferred through the Purkinje fibers to the cells of the ventricles. This leads to the rapid depolarization of the ventricular cells resulting in the contraction of the ventricles to pump the blood to the lungs and the other parts of the body [2].

1.1.2 ECG signal procurement

An ECG signal is obtained using 12 leads. The procedure starts by attaching 10 electrodes, to certain parts of the chest and limbs. Of the 10 electrodes, one is attached to each arm and each leg and the remaining six are attached to the chest. The electrodes play a vital role in detecting the voltage change through different viewpoints of the heart. The right leg electrode is commonly known as the earth electrode while the other limb electrodes are used to take the measurements of the voltage changes. Out of the twelve leads in the system, three of them are used to measure the electrical potential between the three electrodes on the limbs. These leads are known as standard leads and are titled Lead I, II, and III. All three of these leads are bipolar, meaning that each of them needs two of the three electrodes attached to the limbs to measure the electric potentials. Lead I, II, and III measure the potential difference between the electrodes placed on the right and left leg, right arm, and left leg, and left arm and left leg, respectively. Figure 1.4 shows the placement of these leads forming an Einthoven triangle [1].

The process also contains three Goldberger leads known as augmented limb leads. These three leads are unipolar and are titled as augmented voltage right (aVR), augmented voltage left (aVL), and augmented voltage left foot (aVF). These leads take

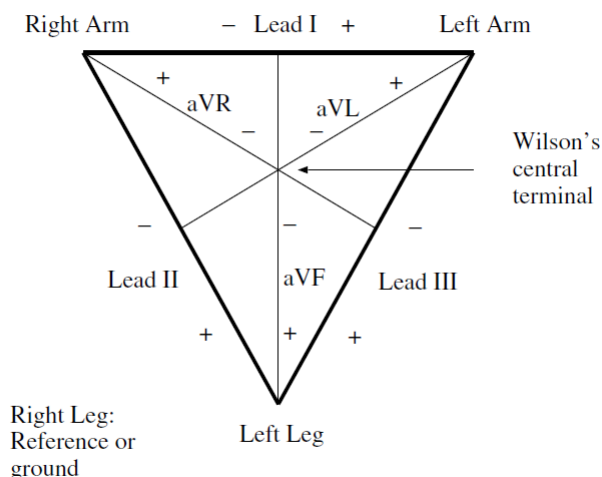


Figure 1.4: The Einthoven triangle formed by limb electrodes and the six leads [1].

one of the electrodes as the positive pole and the mean of the measurements from the other two electrodes as the negative pole. These leads are necessary to measure the conditions of the upper right side, upper left side, and the inferior wall of the heart. The placement of these three leads is also shown in Fig. 1.4.

The six electrodes on the chest are used to obtain measurements for the leads V1, V2, V3, V4, V5, and V6. Figure 1.5 shows the position of the electrodes on the chest. For each lead, the corresponding chest electrode serves as the positive poles. The negative poles are obtained by averaging the measurements of voltage from the three limb electrodes. Thus, the value of the negative pole remains equal for all six leads. The QRS vectors detected by leads V1, V2, and V3 show negative peaks while V4, V5, and V6 produce positive peaks [5]. This is because V4, V5, and V6 are placed closer to the apex of the heart and on the left side of the apex while V1, V2, and V3 are placed on the right side of the apex.

1.1.3 Irregularities in the ECG signal

Arrhythmia is the term given to abnormalities in the heart [1]. If the heart rhythm is irregular or the heart rate is reduced or elevated due to irregular electric activity of the heart then this is regarded as a loss of rhythm of the heart and is also titled arrhythmia [4]. Arrhythmia is mainly caused by Ectopic foci [4] or abnormal beats. The production of such beats results in different types of arrhythmia like atrial, junctional, and ventricular tachycardia, fibrillation, and flutter. Ectopic beats are abnormal electrical impulses caused by significant damage to the SA node of the heart. SA node is the

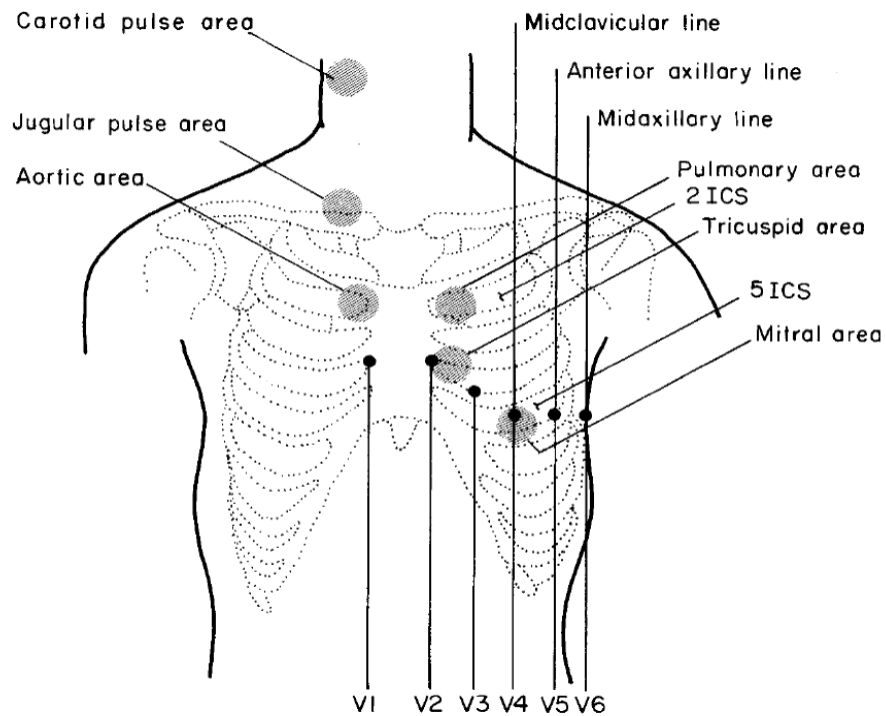


Figure 1.5: The placement of leads on the chest [1].

natural pacemaker of the heart stops working and so the pace making action is taken over by the AV node. This fails to generate any impulse in the atrial region and so the atria do not pump the blood into the ventricles and the natural rhythm of the heart is distorted. Ectopic beats are mainly of three types, namely, premature ventricular contraction (PVC), premature junctional complex (PJC), and premature atrial contraction (PAC).

Atrial tachycardia can also be regarded as fast contraction and relaxation of atrial muscles. Having three or more continuous atrial premature contractions is regarded as atrial tachycardia. The P waves are usually hidden after the T wave occurs and so it is quite easy to be detected. It produces an atrial beat rate of over 140 BPM [4]. Atrial fibrillation (AF) is regarded as a swift and nonuniform contraction of the atria. In AF, the SA node does not produce any electrical impulse to start the cardiac conduction process. The process starts somewhere else in the atria such as the AV node or the nearby pulmonary veins and the signal spreads rapidly throughout the atria. Due to this, the walls of the atria start to vibrate very fast and hence they are not able to pump blood into the ventricles properly. The beat rate for AF is up to 600 beats per minute [4]. Atrial flutter is quite like atrial fibrillation, however, in atrial flutter the signal is conducted through the atria in a fast but regular manner [4].

Junctional tachycardia usually consists of three or more premature junctional contractions [4]. Here, the AV node acts as the pacemaker of the heart due to the failure of the SA node to fire. It can be detected easily as, after the QRS complex, the P waves produced are inverted.

Ventricular tachycardia consists of at least three or more premature ventricular contractions [4]. The QRS complexes are wider than normal and the beat rate is produced in greater than 100 beats per minute [4] but can reach up to 250 beats per minute [5]. In this case, the ventricles are not full of blood when they contract and so the supply of blood to the body suffers and can result in death. Ventricular fibrillation occurs when the SA or AV fails to send electrical signals to the walls of the ventricles. This makes the muscles of the ventricles to vibrate very fast instead of pumping the blood normally. This is a major reason for cardiac arrest and the rhythm of the heart must be mended quickly using a defibrillator.

1.1.4 Artifacts in ECG signal

The ECG signal obtained from an individual contains a lot of noise which makes the R-peak detection very challenging. The frequency band of the ECG signal is between 5 Hz to 35 Hz [6, 7]. Within this particular band, most of the information regarding the QRS complex is available. However, within this frequency band electromyogram (EMG) is also found [6] which in most cases overlaps the ECG signal. Therefore, it is difficult to obtain a full ECG signal. Most of the common sources of noise are as follows:

- Powerline interference is mainly of 50 or 60 Hz [1]. It is a result of the inappropriate grounding of electrodes. This is a high-frequency noise that produces multiple spikes in the ECG signal if not a sinusoid [1]. Power line interference can be easily removed using bandpass or notch filtering. Figure 1.6 shows a section of the ECG signal contaminated by powerline interference.
- Motion artifacts are low-frequency noises produced by the movement of any sort, for example, breathing, coughing, arm, and leg movement [1]. This noise can be removed using bandpass or low pass filters. Figure 1.7 shows a section of the ECG signal contaminated with motion artifacts.
- Baseline wander is a low-frequency artifact in the ECG that is the result of breathing, electrically charged electrodes, or muscle movements. In the resultant cases, the baseline drifts higher or lower than the zero lines and so might

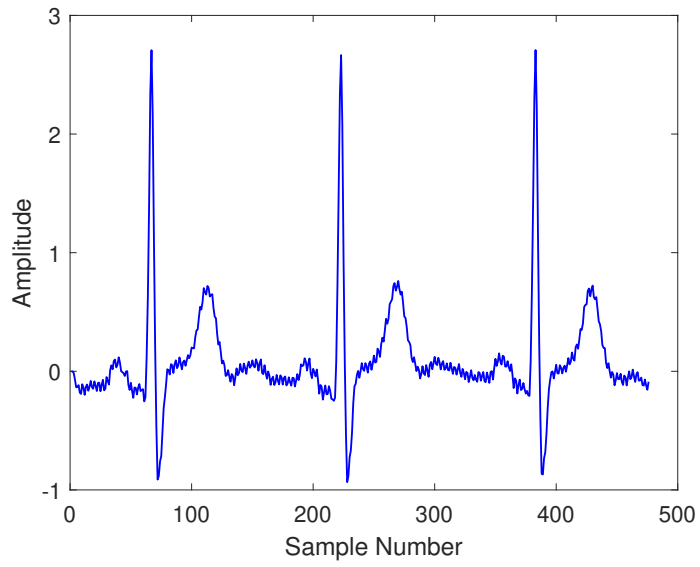


Figure 1.6: ECG contaminated with powerline interference.

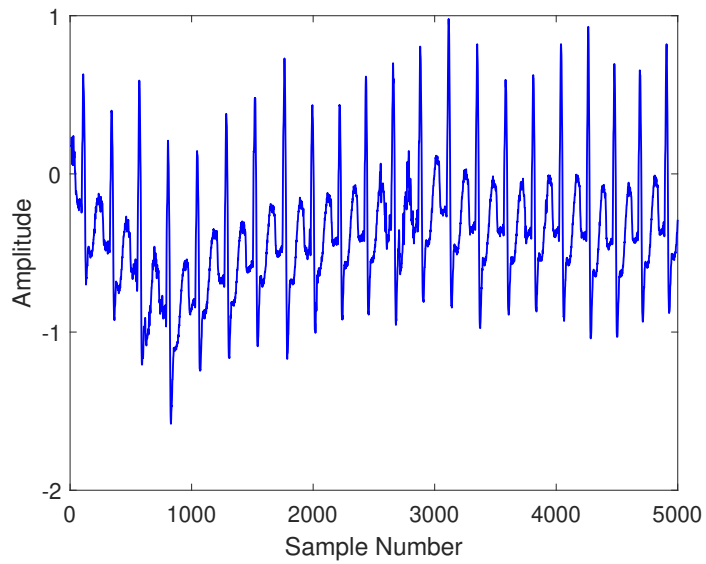


Figure 1.7: ECG contaminated with motion artifacts.

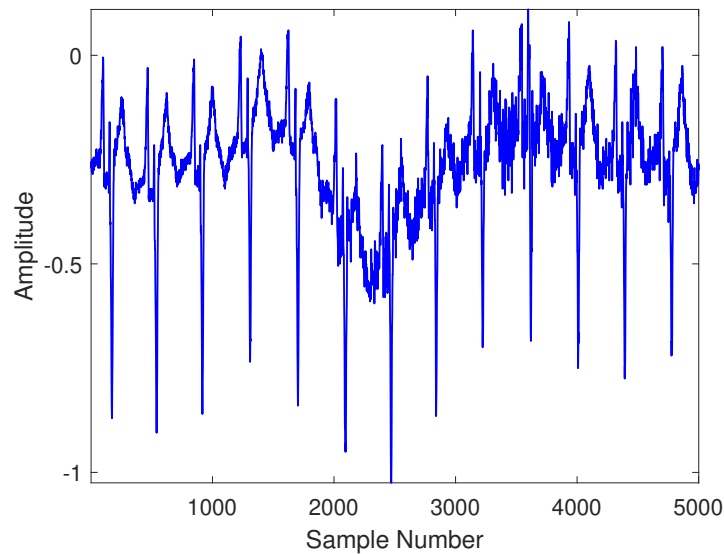


Figure 1.8: ECG contaminated with baseline wander.

result in distortion of desired results. The baseline wander has a frequency between 0.5 to 1 Hz. Figure 1.8 shows a section of the ECG signal that has baseline wander.

- Electromyogram (EMG) is a biomedical signal that contaminates the ECG signal. The frequency range of the EMG signal falls between 10 Hz to 500 Hz with most of its power spectrum falling between 20 to 200 Hz [6]. EMG signal is very hard to remove with any type of filtering as it overlaps the ECG signal partially within its frequency band. Figure 1.9 shows a section of the ECG signal contaminated by the EMG signal.

1.2 QRS Complex and Ectopic Beat Detection

QRS complex and ectopic beat detection have been quite an important study as certain anomalies in the heart can be detected to provide doctors and patients with the proper diagnosis. While external noise interferes with proper detection, arrhythmia also adds to the difficulty of identifying QRS complexes and ectopic beats.

1.2.1 Problems with automatic QRS detection

QRS detection has been quite an important study as it can detect anomalies in the heart to provide doctors and patients with the proper diagnosis. However, the problems with proper and accurate detection of peaks persist. The main reason behind it

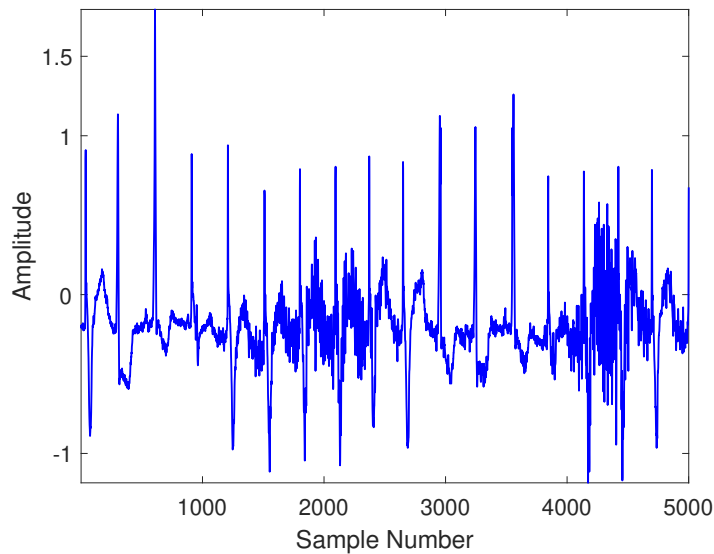


Figure 1.9: ECG contaminated with EMG signal.

is irregular intervals between peaks, irregular peak structure, the large amplitude of P and T waves, and noise. To mitigate the noise in the ECG signal, several filtering techniques such as bandpass, moving average, median, and derivative filter have been employed. The problem with the use of such filters is that these filtering techniques either fail to reduce the noise or cancels much of the information of the ECG signal. The R-peak is a high-frequency component of the QRS complex and has a prominent sharp amplitude and can be detected easily if not reduced by filtering. However, selecting an abnormal frequency band using filters can diminish the information of the R-peak and reduce its amplitude. Linear and non-linear transformations such as wavelet transform, Hilbert transform, and Empirical mode decomposition can reduce the noise and aid in automatic detection making it more successful in capturing the peak information. However, irregular peak structures have provided a challenge even for the best of the transformation techniques. Therefore, solving the problem of detection of peaks is of the utmost value in medical science as the heart is considered as the main organ of the body.

1.2.2 Background of automatic peak detection in ECG signals

The acquisition of ECG using the 12-lead is the best method available to date. However, the automatic detection of peaks in an ECG signal remains an important area of research. The rule that Pan and Tompkin [7] established marked the era for adaptive thresholding with low computational complexity and set a benchmark for the task of QRS complex detection using programming languages. The algorithm is quite simple

and easy to implement and thus is used widely even now. The process involves preprocessing the signal with a bandpass filter, finding its derivative, squaring the derivative, and finally, the use of a window of 150 ms to extract the QRS complex [7]. The process starts with preprocessing the signal with a bandpass filter of bands 5 Hz as a lower band and 15 Hz as a higher band. This removes most of the unwanted artifacts in the given signal and thus derivative filtering can now be done to get an overview of the slope of the QRS and P and T waves. The signal then goes through a non-linear transformation [7] which is squaring. Squaring removes the negative peaks and enhances the peak values. Finally, a moving average window of 150 ms is used to remove the high-frequency artifacts from the signal [7]. The main process of peak detection begins with setting a fiducial mark for the QRS complex at the positions of all the local maxima with a space of at least 200 ms in between peaks found in the signal after the bandpass filter is used. The threshold is initialized with values of two thresholds for signal peaks and noise peaks. It takes about two seconds for this initialization which analyses samples in the ECG signal and decides the values of the two thresholds. The algorithm works as follows:

- If the current peak is greater than the threshold of the signal, then it is regarded as a signal peak, and the signal level is changed to:
 $0.125 * \text{current peak} + 0.875 * \text{signal peak}$.
- If the current peak is between the threshold of the signal peak and the noise peak, then it is regarded as a noise peak, and the noise level is changed to:
 $0.125 * \text{current peak} + 0.875 * \text{signal level}$.
- The signal threshold is then changed to:
 $\text{noise level} + 0.25 * (\text{signal level} - \text{noise level})$
- Noise threshold is changed to $0.5 * \text{Signal threshold}$.

A search back is always initiated if no peaks are found within the $1.66 * \text{R-R interval}$. The R-R interval here depends on two values, one is the average of the last 8 peak intervals and the other is the mean of the eight most regular R-R intervals that fall between 92% and 116% of the average R-R interval. The value of the threshold is lowered to 50% of the signal threshold. A search back is initiated at this stage and if still no peak is found then the highest amplitude around a certain position is selected as a peak. However, in cases of multiple detections within a certain period which is shorter than the average R-R interval, the algorithm considers that a peak can not occur within 200 ms of the last one and the peak is solely discarded thus minimizing false detection. Then again if a peak occurs within 360 ms of the last peak which is

also more than 200 ms, then the slope of the wave is checked. If it is found that the slope of the wave is less than half the previous QRS complex, then it is discarded as a T-wave.

The algorithm in [7] was further enhanced by Hamilton and Tompkin [8]. This paper has the same preprocessing stage and the search back stage as Pan-Tompkin's algorithm. However, the decision making stage is quite different. The focus was more on the optimization of decision rules for the decision process. The adaptive threshold is chosen by mean, median, or iterative peak level of which the median estimator was found to be the best in terms of fewer false peak detection and detection accuracy. Overall, with a slight improvement over Pan and Tompkin's algorithm, the efficiency of QRS complex detection and exclusion of false positives were achieved, however, the algorithm still lacks high accuracy because of the ambiguity in threshold placement. Adaptive thresholding detection has certain advantages over other techniques such as it is a high-speed algorithm, occupies a low space of memory, can be realized in real-time detection, and is suitable for portable, wearable, and wireless ECG systems. However, the only drawback of this technique is having a low-accuracy in detection of QRS complexes and so the use of such technique results in high number of false positives [9]. The algorithm described in [9] has shown better results at detection than Pan and Tompkin's algorithm. The difference between the two is the decision-making stage where some improvements were made to enable the user to detect peaks more accurately. Algorithms available in [10–12] also use bandpass filtering and derivative operations. In [11], the QRS region is found by squaring the double differenced signal and then using a threshold. The R-peaks are found by calculating the maxima and minima of each QRS window then finally initiating a search back for missed peaks and the elimination of false peaks. In [12], single difference operation is used which considers that a QRS region is around 140ms long and uses low pass filtering of a cut-off frequency of 100 Hz to eliminate high-frequency noise. The process is quite simple as it does not contain any higher-order mathematical calculations. An adaptive second-order derivative method was introduced in [13]. The algorithm uses second-order derivative filtering of local weights along with bandpass filtering and logarithmic transformation to denoise the signal and detect peaks. This method can be used in real-time and can be considered as an upgrade of all double differencing algorithms.

Another detection technique employed by several authors is the one that applies wavelet transform. This is a relatively newer technique of ECG denoising and with great

amount of research conducted that show promising results. The advantage of this method is that it is a suitable method for locating different waves with typical frequency characteristics. A QRS complex lies between 10 Hz to 25 Hz [14], and so, in most algorithms, a bandpass filter is used to capture these features of the raw ECG signal. The bandwidth chosen to optimize the extraction varies. For example, Pan-Tompkin's algorithm uses a bandpass filter of 5 to 12 Hz [7] and others use high pass filters, parallel high pass and low pass filtering, adaptive filters, empirical mode decomposition and several others. The main motive is to reduce the noise while keeping the high-frequency details of the QRS intact. The bandpass filter cannot adapt to the sudden variations in the bandwidth in the frequency domain of the QRS [15]. The continuous wavelet transform is the output of a bank of bandpass filters whose center frequencies and bandwidths vary depending on the dilation parameter [15]. Due to the variation in bandwidth, the resolutions are different for various scales [15]. However, one prime disadvantage of such a system is its complexity and the extensive usage of memory. To solve this problem, the dilation parameter of the CWT is discretized to a positive integer which is a power of 2. This is called dyadic wavelet transformation. Dyadic or discrete wavelet transform uses a mother wavelet which is then scaled and shifted to produce a daughter wavelet [16]. This wavelet is convoluted with the signal to capture the most prominent features of the signal. At high frequencies, the wavelet provides good time resolution and at low frequencies, it provides good frequency resolution. Discrete wavelet transform is a linear transformation of non-stationary signals. It is a handy tool that can recognize sharp changes in the input signal depending on the mother wavelet used to analyze the signal. In this paper, basically the technique of wavelet transform use filter banks to decompose the signal into different frequency sub-bands and then reconstructing the signal. Each level uses a filter bank consisting of a high-pass and a low-pass filter followed by decimation by 2 for both filters. The signal obtained from the high pass filter is called the detailed signal and from the low pass filter is called the approximate signal [17]. Therefore, another level is established where the signal from the low pass filter after decimation is fed into another filter bank which is approximately half the size of the first level filter bank. Here another high pass and low pass filter are used in parallel like stage one and the signal is again divided into another sub-band consisting of another detailed signal and another approximate signal after decimation by 2 again. This goes on for 'n' number of stages unless a suitable output is obtained.

Wavelet packet decomposition is used in [17]. Wavelet packets are waveforms indexed by three parameters of position, scale, and frequency [17]. In the wavelet decomposi-

tion process, the signal is divided into approximation signals and detail signals. The information lost between successive approximations can be found in the detail coefficients [17]. The input signal is divided into several levels with each level having approximation coefficients and detailed coefficients. In [18], the author uses eight levels of decomposition to explain at what frequency range does the QRS falls. The highest correlations found were for frequencies between 4.062 Hz to 32.5 Hz. Similar work has been done in [16] where again eight levels of decomposition were used and most of the energy of the QRS was found out in stages 3, 4, and 5. In addition to this, P and T waves, which are prominent unwanted components of the ECG signal were found to be in the 6th and 7th stages with baseline wander occurring in stage 8. Further work had been done in [19] which deals with 50 Hz powerline interference removal using wavelet transform. Haar-wavelet was first used in the algorithm which reduces the noise but also distorts the signal into something resembling square waves. Secondly, the db4 wavelet was used which showed very low distortion and was comparatively better than Haar-wavelet for ECG signals and that was further confirmed in [19]. In [20], the resultant changes of four different types of mother wavelets were displayed which are Haar, Db3, Quadratic spline, and Cubic spline wavelets. Amongst these Db3 and Cubic spline wavelets have a good correlation to QRS structure. Similarly, in [21], the author used a new prototype of a quadratic spline wavelet to test the denoising of the signal. The number of levels used was 5 and the energy of the QRS at levels 4 and 5 was found to be very low. For levels 1 and 2, the coefficients displayed high-frequency noise. Therefore, level 3 was selected to resemble the QRS complex. In [22], it was also stated that the energy of QRS complexes lies within 5 to 22 Hz with 5 levels of decomposition for a maximum frequency of 180 Hz [22]. In [23], the author emphasized on eliminating Gaussian noise. According to the author, this noise interferes with the signal to a high extent and makes the extraction of the clean signal very difficult. The author used Daubechies wavelets to filter the signal. These wavelets are orthogonal and have a maximal number of vanishing moments representing higher degree polynomial functions [23]. These brands of wavelets were selected due to their high cross-correlation with QRS complexes. The algorithm in [23] uses 6 stages. The detail coefficients of the unwanted noise components were set to zero after transformation. The work done confirms that wavelet transform can be used to separate different frequency components and that the unwanted components can be removed by setting detailed coefficients of the components to zero. Inverse wavelet transform can be applied to obtain the noise-free signal [23]. A more accurate way of identifying peaks was discussed in [24]. The algorithm combined wavelet denoising and Teagar energy window-based approach to perform automatic peak detection. An

enhancement to a basic wavelet transform can also be observed in [25]. The wavelet denoising was made tuneable for menacing ECG records to make the detection of peaks simpler.

Hilbert transform is another method that is used widely for R-peak detection. It is an odd function [26] and so it will have a zero-crossing exactly at the points where the original signal has a peak and a peak where the original signal has a zero crossing. Therefore, the first derivative of the signal is always taken ahead of the Hilbert transform as a peak in the original signal represents a zero crossing in the derivative which in turn represents a peak in the Hilbert transformed signal. In [26], a method of using the first derivative of the ECG signal followed by its Hilbert Transform is implemented. Similarly, [27] uses approximately the same techniques. Both algorithms use the wavelet transform to eliminate noise rather than using a standard bandpass filter which gives better accuracy for noise reduction. Moreover, each of the methods in [26, 27] have different decision-making rules regarding adaptive thresholding. In [26] the threshold was selected by taking the peak amplitudes of the local peak and finding out the maximum amplitude of the Hilbert transform envelope. In [28] and [29], a combination of Hilbert and wavelet transform is employed. The algorithm in [28] employs two thresholds which are Up Limited (ULT) and Down Limited Thresholds (DLT) [28]. The signal is then processed by these two values, separately, and two sets of peaks are detected, one with values higher than the ULT and the other which is higher than the DLT.

Another effective method for R-peak detection is Empirical value decomposition [30]. A new method of removing the baseline wander was used using a fast Fourier transform. However, the fact remains that baseline wander is a low-frequency component of frequency 0.5 Hz to 1 Hz and can easily be removed by using a high-pass filter or median filter. The high-frequency noise was targeted like the powerline interference. This component can be found in one of the lower order IMFs however, if most of the lower order IMFs are removed then the QRS will be distorted as the QRS is also a high-frequency component because of its sharp changes. To counter this, an efficient method was proposed in [30]. A similar method was also implemented in [31], however, that method takes a non-linear transform into account after finding IMFs of the baseline stabilized signal. Only the first three IMFs were used in [31]. Another famous algorithm is the Hilbert Huang transform (HHT) which uses EMD with Hilbert transform to attain the desired accuracy of detection. The main method combined EMD and Hilbert transform to generate time-space filtered signals [32]. The ECG

signal was divided into its IMFs as before but with a new thresholding technique. The first to the third IMFs were cleaned with a hard threshold to remove all high-frequency noises. The last scales of IMFs were eliminated or made zero as it only contains the baseline wander. Hilbert transform was applied to each of those IMFs as EMD was effective in reducing the noise [33]. An enhancement to EMD was presented in [34] in the form of complete ensemble empirical mode decomposition which lessens the number of shifting operations by almost half and therefore reduces the computational complexity [34].

Adaptive filter-based approach to ECG signal denoising is described in [35] with an overview of the performance of different types of adaptive filters. Moving median filters were used in [36] and mean-median filtering along with DWT was used in [37] to remove the baseline wander. This yields better results for noise cancellation than other methods. The use of moving average filters was presented in [38] to suppress power-line interference. Machine learning approaches to detect QRS are found in [39–44]. These algorithms use deep learning and convolution neural networks to classify the beats and the noise. In [45, 46] algorithms based on simple learning and transformations that can be easily implemented without using machine learning were introduced. Kalman filters were used for QRS detection in [47] while they were used along with adaptive thresholding to detect peaks in [48].

1.2.3 Motivation

Cardiovascular diseases have been one of the leading causes of death all over the world. CDC reported in 2011 that a third of the patients who die in the United States alone are heart patients [49]. With the growth in population in the world, doctors and nurses in many regions are often overwhelmed with the number of heart patients. Delays in diagnosis can lead to cardiac arrest and fatality in the older population. Professionals often have to work overtime studying the ECG signal very carefully to denote any ectopic beats or arrhythmia. Sometimes due to lack of experience or fatigue proper analysis is not given correctly resulting in permanent heart damage or even death. Therefore, to analyze the ECG signal fast and accurately is a very important task. Moreover, cost reduction is a key issue. Continuous monitoring for cardiac patients is expensive to implement and the time it takes to read a record of 30 minutes is quite high. Therefore, automatic QRS detectors are an area of interest for many biomedical sectors. There are certain advantages to using such systems. Firstly, it eases the workload of physicians as they can use the system to monitor multiple

patients at a time in the same amount of time, they would have used to study one recording from one patient. Secondly, the diagnosis is instant and does not require anyone to wait for days before they get their results. Thirdly, if such systems can be used in mobile devices then patients do not have to be moved and an ECG test can be performed at home. All these advantages give automatic detection an edge over conventional visual observation and make QRS detection algorithms a much-needed area of research.

1.3 Thesis Contribution

This thesis presents automatic peak detection algorithms for ECG signals. It consists of three main algorithms:

- A novel method of QRS detection using multidimensional thresholds and statistical false peak elimination.
- Single-channel QRS detection using discrete wavelet transform and median denoising with adaptive multilevel thresholding.
- QRS detection using adaptive multilevel thresholding, segmentation, and false peak elimination.

First, various ways of noise reduction techniques are explored. Several techniques are implemented, e.g., adaptive filtering, empirical mode decomposition, median filtering, average filtering, bandpass filtering, wavelet transform, and derivative filtering. It is found out that none of these noise reduction techniques could reduce the noise completely, however, some of those techniques could minimize the noise enough for adaptive thresholds to detect the peaks. According to [6], the ECG signal can be best captured if the frequency bandwidth is taken below 35 Hz, considering using a low-pass filter, while according to [7], the frequency bandwidth is taken above 5 Hz when a highpass filter is considered. It was found out that none of the techniques except for bandpass filters can perform the task to select the exact frequency range of 5 to 35 Hz. Similarly, moving average filter was found to be effective at minimizing the interference from other biomedical signals such as electromyography (EMG). For the first algorithm, we have considered median filters to cancel the baseline wander and minimize the P and T waves. In addition to this, a moving average filter is employed to diminish other high-frequency noises and the EMG signals. A new method of segmentation and false peak elimination, based on the characteristics of the ECG signals, is also proposed to delete false peaks that result from the EMG and any other high-frequency noise components remaining after filtering. A search back algorithm is also

proposed that can detect peaks with lower amplitude than the ones that have been detected.

In the second proposed method, we have investigated multilevel thresholding. The idea of using multilevel thresholds is available in [50]. Therefore, in this thesis, discrete wavelet transform is used up to only three levels along with adaptive multilevel thresholding to separate the R-peaks and the ectopic beats from the noise peaks. This algorithm consists of discrete wavelet transform and median filtering along with smoothing to preprocess the signal. Later, two levels of adaptive thresholds are devised and varied automatically along with one nonadaptive threshold. The search back stage is also altered to perform better in detecting missed peaks.

The third proposed method of the research consists of a combination of the two earlier algorithms with slight modifications to achieve better detection. For this purpose, segmentation and false peak elimination are combined with two levels of adaptive multilevel thresholding to create one algorithm which reduces the number of stages that are present in the first algorithm and also route out the need for segmentation while performing search back. The results achieved show that this algorithm is highly robust.

1.4 Thesis Objective and Outline

The objective of this thesis is to find an efficient way of detecting peaks such as R-peaks in the QRS complex, and ectopic beats such as the premature ventricular contractions (PVCs), premature junctional complexes (PJC), and premature atrial contractions (PACs) using statistical and adaptive thresholds. The motive is to maximize the number of true detections of R-peaks and to make the detection of peaks computationally simple and low cost while achieving high accuracy in proper detection. The reasons for this are as follows:

- The information of the peaks is reduced significantly if a proper frequency band is not chosen for filtering.
- Proper detection is hard to achieve due to irregularity in peak structure and peak-to-peak interval.
- Linear and nonlinear transformations distort the ECG signal.
- Most of the algorithms developed till now emphasize filtering more than thresholding.

This thesis is divided into five chapters. Chapter 1 consists of the introduction that briefly considers the importance of the research, the problems associated with automatic detection, and the previous work associated with the study. Chapter 2 represents the first proposed algorithm based on a new method of automatic segmentation of the ECG signal and statistical false peak elimination. This method breaks down a long ECG record into smaller segments and processes the peaks of each segment in contrast to the mean peak-to-peak intervals of that segment. Considering the standard deviation of the peak-to-peak intervals and the maximum number of beats achievable per second, the algorithm chooses the actual peaks and eliminates the peaks due to noise. A statistical search back method is also devised as the post-processing stage to detect low amplitude missed peaks by taking into consideration the average peak-to-peak interval and the standard deviation of the peak-to-peak intervals. This stage also uses automatic segmentation. Chapter 3 presents the second proposed method, a new method of adaptive multilevel thresholding using discrete wavelet transform, and median filtering. Discrete wavelet transform and median filtering are used to reduce the high-frequency and low-frequency noises, respectively. Adaptive multilevel thresholding is used to detect the R-peaks and the ectopic beats. Chapter 4 presents a proposed method that combines adaptive multilevel thresholding, segmentation, and statistical false peak elimination. This method can vary the amplitude thresholds adaptively with the change in the amplitude of signal peaks to enhance detection performance. Segmentation and statistical false peak elimination can better adapt to remove false peaks and find the actual ones if paired with adaptive multilevel thresholding. The search back algorithm here does not use segmentation or rely on the standard deviation of the peak-to-peak intervals as more true positives are detected and false peaks are eliminated beforehand. Lastly, the conclusion and future work is provided in Chapter 5.

Chapter 2

A Novel Method of QRS Detection Using Multidimensional Thresholds and Statistical False Peak Elimination

2.1 Introduction

The electrocardiogram (ECG) is a non-invasive test [13] for the heart which is conducted by placing electrodes on the chest to record the electrical activity of the heart [14]. It contains P waves, QRS complexes, and T waves. The signal obtained from an individual has large amounts of noise components which make the R-peak detection very challenging. R-peaks are prominent features in the ECG signal, however, due to noise, they are quite often suppressed and cannot be detected properly without removing the noise contaminating the sample. Two other problems encountered while performing peak detection is the irregularity of peak structure and irregularity of peak-to-peak intervals. This feature is found in patients having a condition called arrhythmia which is discussed in Chapter 1. In this chapter, we present a simple statistical approach for detecting QRS without using any computationally intensive transformations. Here, we propose a novel technique based on median and moving average (MA) filters, segmentation and mean of R-R interval as a threshold. The use of median filters stabilizes the baseline wander and minimizes the amplitudes of the P and T waves while moving average filtering gets rid of high amplitude electrical noise.

2.2 Data Acquisition

The proposed method is evaluated on two distinct databases, namely, the MIT-BIH arrhythmia database [51], and the Fantasia database [52] from PhysioNet [53] which is an open source for physiological signals. The MIT-BIH arrhythmia database has a variety of records with diversity in morphological changes that better suit better for the evaluation. The records contain both high and low-frequency noise and artifacts and P and T wave interferences. The database provides 48 ECG records of length 30 minutes each with a sampling frequency of 360 Hz and an 11-bit resolution over ± 5 mV range [51].

The records were collected from 25 male and 22 female individuals between the age of 23 to 89. Five leads have been used to collect the data which are MLII, V1, V2, V3, and V4. Now, each record would use two of the five leads to collect the data that is each record has two channels which can be used for evaluation purposes. For our research, we have focused on channel MLII which is widely used and is used to record directly from the chest. The annotations for the database are decided and placed by cardiologists.

The Fantasia database consists of forty recordings from 32 individuals between age the 21 to 85. Here, the channel I records the breathing rhythm and so the channel II is used for the purpose of this study. The sampling frequency is 250 Hz and each record is two hours long [53]. The annotations for this database are checked by visual inspection.

To demonstrate the performance of the proposed method and compare that to the state-of-the-art methods we have also included 20 records from the European ST-T Database. This database contains 90 records from 79 individuals with a sampling frequency of 250 Hz over ± 10 mV range [54]. The annotations in this database are verified by two cardiologists separately.

2.3 The Proposed Method

Unlike most algorithms in the literature, this method is formulated using three different stages. Firstly, as shown in Fig. 2.1 the first stage is the preprocessing stage to filter out the unwanted noise and artifacts and minimize the effects of P and T waves. The function of the second stage is to break down the ECG record into smaller segments

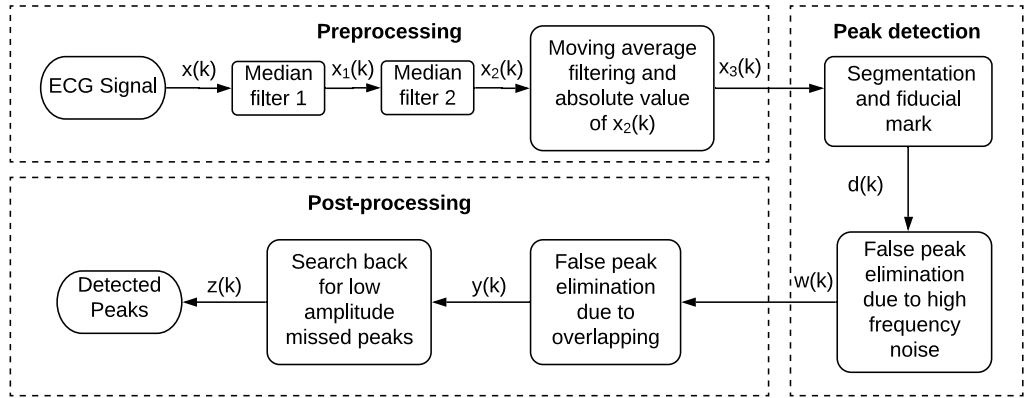


Figure 2.1: Block diagram of the proposed method.

and to perform peak detection on each of those segments, separately. This stage is referred to as peak detection in Fig. 2.1. Each record is divided into equal segments of maximum 25000 samples per segment and an amplitude axis threshold is used to eliminate very low amplitude peaks. The mean difference between adjacent peaks is now calculated and used as a time axis threshold to eliminate any peaks resulting from any residue of high-frequency noises. Lastly, the post-processing stage in Fig. 2.1 is used to link together the smaller segments in the order of their original structure, to cancel any repeated peaks resulting from one peak detected twice at the edge of adjacent segments. A search back sub-stage is finally used to detect any missed peaks by learning from the R-R interval throughout the entire ECG record. Here, $x(k)$ is the input ECG signal, $x_1(k)$ is the signal after passing through the first median filter, $x_2(k)$ is the signal after being passed through the second median filter, $x_3(k)$ is the signal after passing through moving average filter and after absolute value, $d(k)$ is the segmented signal, $w(k)$ is the signal from which false peaks are eliminated due to high-frequency noise, $y(k)$ is the signal from which false peaks are removed due to one peak being detected twice as the signal was divided into smaller segments and $z(k)$ is the final peak detected signal. To reduce the processing time and to improve detection accuracy we have considered each segment to be less than or equal to 25000 samples which is automatically decided in the algorithm itself. The entire work can be classified as being a simple first-order statistical analysis of ECG signal. The proposed method is evaluated over two standard databases and compared with existing state-of-the-art methods.

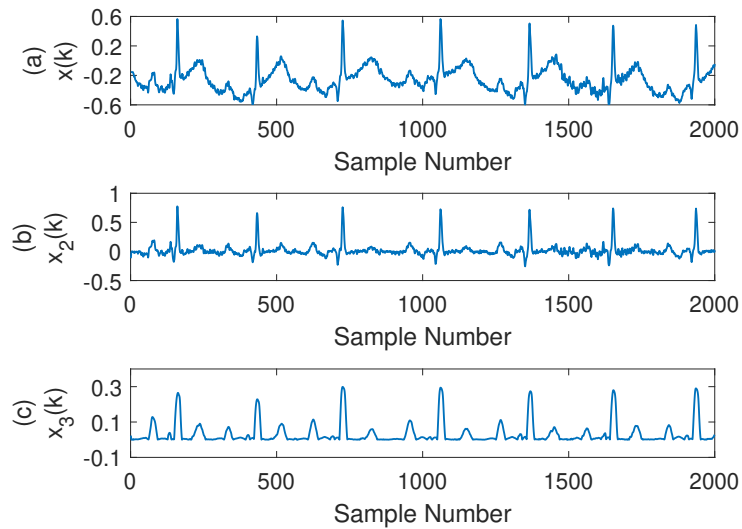


Figure 2.2: Outputs obtained from different stages with y-axis in mV. (a) ECG signal from record 228 of MIT-BIH database, (b) Signal obtained after median filtering, (c) Signal obtained after preprocessing.

2.3.1 Preprocessing

This stage contains two steps to suppress noise and other artifacts in the ECG record. It is constructed out of two median filters and a moving average filter of 20 samples.

Median Filtering

The preprocessing stage kicks off with processing the entire record with two median filters with a window size of the second filter being twice the first filter. The window sizes can be selected to be either, 50 ms and 100 ms, or 100 ms, and 200 ms respectively. This is because P waves occur between 50 to 100 ms before the QRS complex and T waves occur between 50 to 100 ms after the QRS complex. Combining these two median filters in a cascade not only diminishes the P and T waves but also eliminates the baseline wander. Any other low-frequency noise that might be in the record will also be minimized if not fully eliminated. To illustrate this effect Fig. 2.2(a) shows the original ECG signal from records 228 of MIT-BIH arrhythmia database with noise and Fig. 2.2(b) shows the effects of median filtering.

Moving Average Filtering

A moving average filter is employed to suppress the high-frequency noises in the ECG record. Conventional methods use a variety of filters for this purpose. However, using FIR bandpass filters can reduce the peak information significantly [8]. To avoid this a moving average (MA) filter of 20 samples is utilized. Figure 2.2(c) shows the signal after passing the signal through the moving average filter. The filter reads 10 samples to the left of the designated sample and 9 to the right and calculates the average of these 20 samples to replace it at the position of the designated sample. This reduces the EMG and other high-frequency noises significantly without destroying the peak information. However, one drawback of such filter is that it cannot eliminate the noise fully but rather suppress it of a smaller value. The peak detection stage is thus designed to deal with this problem. The filter also provides a smooth envelope for the ECG which makes the R-peaks prominent. The absolute value of each of the samples is then found to account for premature ventricular contraction (PVC) which lay below the x-axis for most signals. PVCs are ectopic beats produced by the ventricles of the heart that interferes with the rhythm of the heart. They are the main reason for the heart to initiate ventricular flutter or to skip a beat. The detection of the PVCs is very important as seeing their shapes and amplitudes doctors can predict the abnormality of the sequence of heartbeats and therefore, diagnose a disease properly. In our algorithm, the PVCs are also considered as beats replacing R-peaks when the heart struggles to beat properly.

2.3.2 Peak detection using statistical peak-to-peak interval analysis

This stage consists of two steps, segmentation, and false peak elimination where the ECG is divided into smaller segments depending on how many samples it consists of. Each segment is processed separately to detect peaks. Figure 2.3(a) shows a portion of the ECG signal from record 228. Figure 2.3(b) shows peaks detected on the absolute value of the mean envelope, where the red circles show the peak position and Fig. 2.3(c) shows the detected peaks on the raw ECG signal, where the circles display the peak locations.

Segmentation

After preprocessing is done the record is now divided into segments of m samples each. This can vary according to the length of the record but for better accuracy and

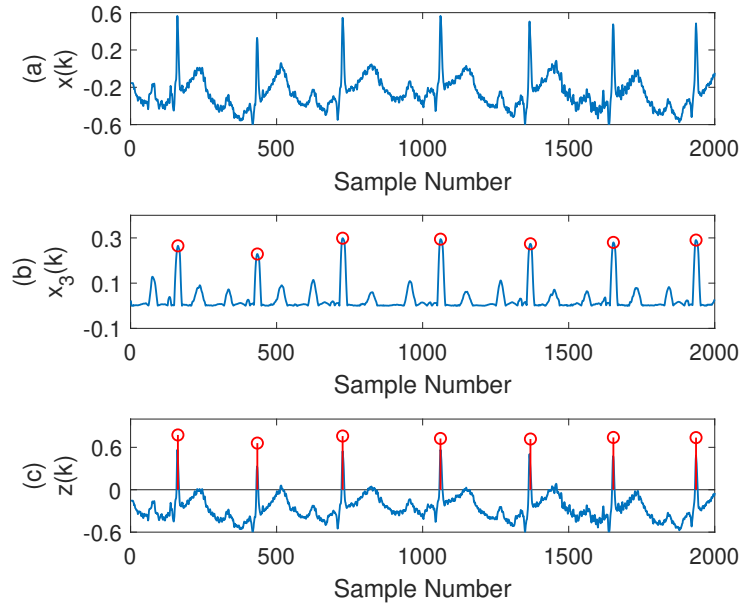


Figure 2.3: Outputs obtained from different stages with y-axis in mV. (a) ECG signal from record 228 of MIT-BIH database, (b) Peaks detected on the preprocessed signal, (c) Peaks detected on the original signal. The circles provided show the detected peaks on the corresponding signals.

low processing time, the number of samples should not be more than 25000. The notion is to process smaller segments to better adapt to the change in morphology of the ECG. To make the division of samples automatic the algorithm is initialized with $\mathbf{R} = [2, 6, 20, 26, 40, 60, 72, 74]$, where \mathbf{R} is the number of total segments to be produced. If the length of the record is equal to 50000 or less, then the number of segments chosen is 2 from vector \mathbf{R} . Similarly, for records with sample numbers less than or equal to 150000, 500000, 650000, 1000000, 1500000, 1800000 and 1850000 the number of segments chosen would be 6, 20, 26, 40, 60, 72 and 74 respectively. For example the MIT-BIH arrhythmia database has 650000 samples for each record and so is divided into 26 smaller segments of 25000 each for our experiment. For the databases we have used in our work no record with more than 1850000 samples were found.

Fiducial Mark and False Peak Elimination

In this step, each segment is processed individually. First, a fiducial mark, \mathbf{W} is created which is a vector consisting of all the local peaks in the segment with a minimum peak separation of 200 ms between peaks. Once this is done, the average amplitude, A , of

all these peaks is calculated using formula,

$$A = \frac{\sum_{n=1}^Q W(n)}{Q}, \quad (2.1)$$

where, Q is the number of total peaks, $W(n)$ is the weight of the vector at position n and n is the position of the peaks in vector \mathbf{W} . We use upper and lower case boldface to denote vectors.

Now, the segment is again processed to detect all the possible peaks with a minimum peak-to-peak interval of 320 ms and an amplitude (y-axis) threshold of C , is found C is a value proportional to A and lies between 70% and 125% of the value of A . This is due to fact that the algorithm depends on learning the peak-to-peak intervals and a huge number of false peaks in the initial detection can throw the analysis out of balance. So, we try to minimize false detections from the beginning to achieve better results.

Once all the local peaks above the amplitude threshold, C is found it is time to select the true positives and eliminate any peak resulting from high frequency noises. Let the vector $\mathbf{L} = [L(1), L(2), L(3), \dots, L(N)]$ represents all the locations of peaks in the segment and let the vector $\mathbf{P} = [P(1), P(2), P(3), \dots, P(N)]$ represents all the peak values and let N be the number of values in vectors \mathbf{L} and \mathbf{P} .

Next, let a third vector $\mathbf{D} = [D(1), D(2), D(3) \dots, D(N - 1)]$ be formed that contains all the peak-to-peak intervals calculated from vector \mathbf{L} , such that,

$$D(n) = L(n + 1) - L(n), \quad (2.2)$$

recalling that n is the position of the values in each vector. Now, the average proportional value, G of the mean of the values in vector \mathbf{D} is formulated using the equation,

$$G = k \frac{\sum_{n=1}^{N-1} D(n)}{N - 1}, \quad (2.3)$$

where, k is equal to 0.8 and 0.5 for low and high morphological change, respectively, and n is the position of the peak values and peak locations in \mathbf{P} and \mathbf{L} respectively.

It is important to note that because there is a minimum interval of 320 ms between

peaks. This because it is hard to achieve a beat rate of over 200 beats/min and there are patients with the ventricular flutter of 200 beats/min [55]. This is because a normal person can only achieve a minimum beat rate of 60 beats/min when awake [56]. If a person has a beat rate of 190 beats/min which means approximately 3.15 beats/s the minimum separation between beats will come at approximately 320 ms between two beats. Furthermore, if the beat rate goes above this threshold it signifies ventricular flutter and not heartbeats.

For example, if a person experiences around 1 beat per second, there cannot be more than two false positives between two adjacent true positives as each peak will be at least 320 ms away from each other. This is shown in Fig. 2.4. Considering this, our false peak elimination was proposed where we compare each value in vector \mathbf{D} with an instantaneous position i , with G . If it is found that $D(i)$ is less than G , then $D(i+1)$ is also compared to G . If $D(i+1)$ is also found to be smaller, then the algorithm guarantees that there is a false peak at position $D(i)$. The location corresponding to $D(i)$ that is $L(i+1)$ will be removed along with $P(i+1)$ and a new interval between the peaks will be established using formula,

$$D(i) = D(i) + D(i+1). \quad (2.4)$$

For example in Fig. 2.4 it is seen that there are two false peaks, (a) and (b) between true positives at 6000 and 7000 ms time marks. The algorithm calculates all the R-R differences and stores in vector \mathbf{D} . Then G is calculated using (2.3) and used to eliminate the false peaks. the interval between (c) and (a) are compared to G and found lesser than G . At this point, the interval between (a) and (b) will also be compared with G and will also be found to be smaller than G . Thus peak (a) will be eliminated from vectors \mathbf{L} and \mathbf{P} . Then the algorithm again compares the interval between (c) and (b) with G and finds it smaller than G . This initiates the comparison of the interval between (b) and (d) with G again. Now, the value of the interval is again found to be less than G and so peak (b) is eliminated.

This goes on for each of the peak-to-peak intervals in the segment and is quite efficient in removing falsely detected peak. However, very high amplitude peaks are excluded from this procedure as PVCs are high in amplitude but closer to their preceding peak than G . The step is repeated for each segment and finally, all the peak locations from all the segments together are obtained and stored in vector \mathbf{U} and their corresponding amplitudes in vector \mathbf{V} . Figure 2.5 shows the effect of using this stage on a segment of record 104. The record contains high frequency noise on some parts and a section of

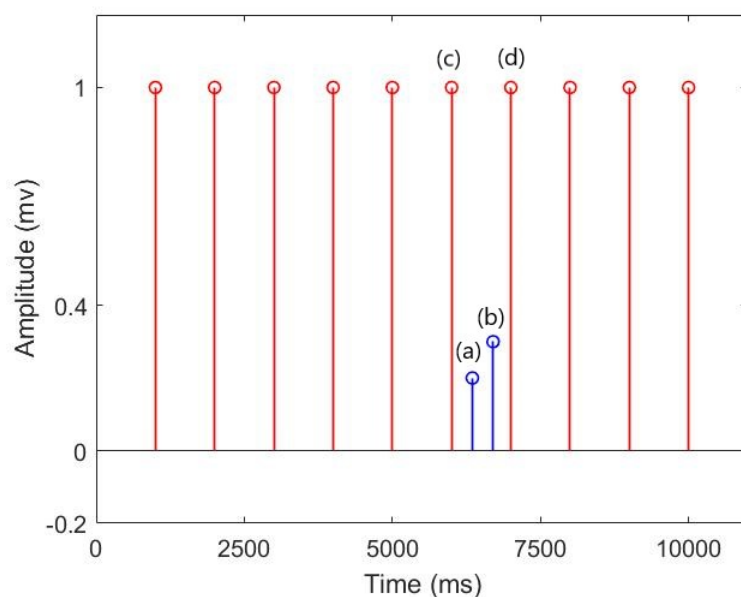


Figure 2.4: False peaks between true positives.

25000 samples are shown which contain high amounts of noise. Figure 2.5(a) displays a peak falsely detected due to high-frequency noise while Fig. 2.5(b) shows the false peak that was eliminated.

2.3.3 Post-processing

The post-processing stage has two steps which are false peak elimination due to overlapping and search back to detect any missed peaks. This stage is important because when the ECG record is divided into segments, there could be a peak at the end or beginning of each adjacent segment that might be detected twice. Also, because some of the records are inconsistent in terms of amplitude, that is the amplitudes might be too high for one part of the record and too low for another part, it is essential to pass these records through the post-processing stage to maximize true detection and minimize false positives.

False Peak Elimination due to Overlapping

After the peak detection stage is complete, the entire record is now analyzed. The vector \mathbf{T} now represents all the peak-to-peak intervals in vector \mathbf{U} where,

$$T(n) = U(n+1) - U(n). \quad (2.5)$$

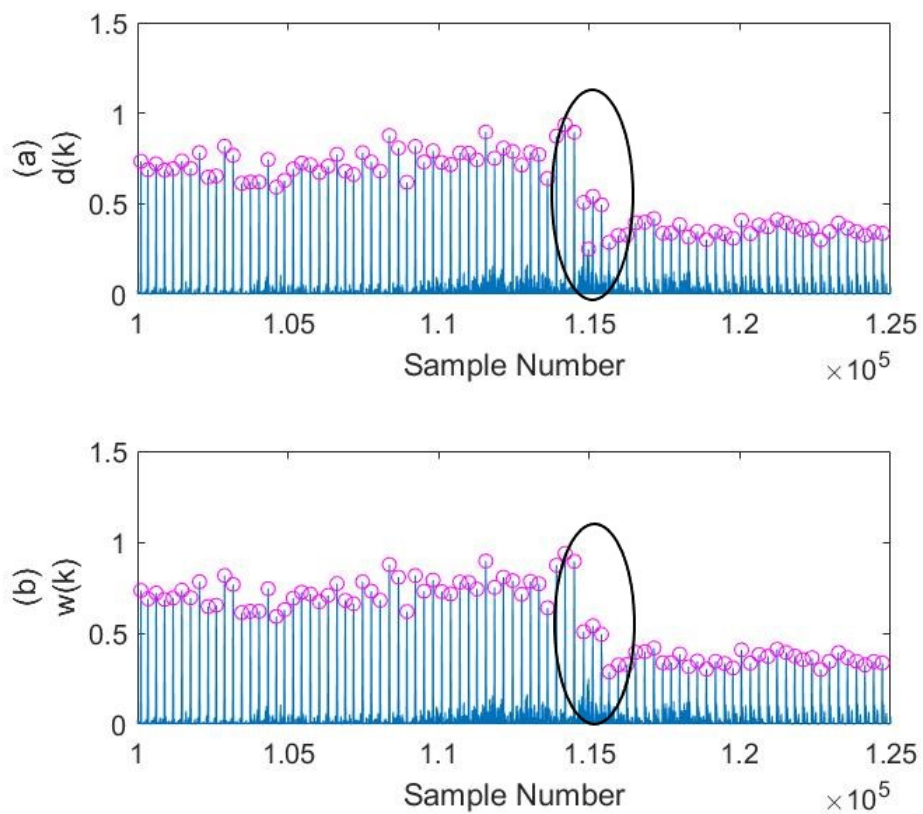


Figure 2.5: False peak elimination in record 104 with y-axis in mV (277-347s) of MIT-BIH arrhythmia database. (a) False peaks detected after preprocessing, (b) False peaks eliminated after assessment.

Here, $T(i)$ and $U(i)$ are the weights of their respective vectors \mathbf{T} and \mathbf{U} . Again a time axis threshold is created by using the formula,

$$H = 0.48 \frac{\sum_{n=1}^{e-1} T(n)}{e-1}, \quad (2.6)$$

where $T(n)$ is the weight of the vector at position n and n is the position of the peaks in vector \mathbf{T} . H is the time axis threshold, e is the number of locations in \mathbf{U} . The full record is processed at a time using this threshold. If an instantaneous peak-to-peak difference, $T(i)$ is less than H then it is regarded as a repeated peak and this peak will be eliminated. Thus, any peak detected twice is now detected only once and so the number of false positives will be reduced further. Table 2.1 provides an overview of the roles of different vectors in the method.

Table 2.1: Vector classification

Vector	Content
R	Number of segments.
W	Locations of local peaks in a segment.
L	Locations of peaks after using amplitude threshold C for a particular segment.
P	Values of peaks after using amplitude threshold C for a particular segment.
D	peak-to-peak intervals using (2.2) for a particular segment.
U	Locations of peaks for the whole after false peaks have been eliminated.
V	Values of peaks for the whole after false peaks have been eliminated.
T	peak-to-peak intervals for the whole record.

Search Back

Finally, when most of the true positives have been detected, there might be a few peaks that the algorithm had failed to detect earlier due to their low amplitudes. So, the segments obtained in the segmentation stage is once again analyzed. Here it is noted that several peaks have been eliminated already as false peaks. Those values are removed from the vectors \mathbf{L} and \mathbf{P} for the corresponding segments and so the new lengths of these two vectors are now f each. Now, vector \mathbf{D} is again formulated but

this time using the new weights in vector \mathbf{L} and by using, (2.2).

This time the amplitude threshold is taken to be B and the mean peak-to-peak interval is taken to be Z for a particular segment,

$$B = 0.1A, \quad (2.7)$$

$$Z = \frac{\sum_{n=1}^{f-1} D(n)}{f-1}. \quad (2.8)$$

The vector \mathbf{L} is further analyzed to find the standard deviation of the peaks. The search back stage will be only triggered if the standard deviation is less than or equal to 100 samples. This is to ensure there is no false trigger as some records are multiform meaning, they have frequent changes in the intervals between peaks. The equation for the standard deviation, S is given by,

$$S = \frac{\sum_{n=1}^{f-1} L(n) - Z}{f-1}. \quad (2.9)$$

Now, the algorithm will account for each peak-to-peak interval and then compare it with the value of the amplitude threshold B and time axis threshold Y , where,

$$Y = 2Z - 4S. \quad (2.10)$$

If the interval between two adjacent detected peaks exceeds the value of Y then the algorithm confirms that there might be a missed peak in this part of the segment. Therefore, all the local peaks with a value greater than B and a minimum interval between the adjacent peak of X is found, where,

$$X = Z - 2S. \quad (2.11)$$

This will result in finding two or more peaks. Once these local peaks are found they are then compared with another time axis threshold M where,

$$M = 0.75Z. \quad (2.12)$$

Only the peaks that have a interval greater than M compared to the established true positive immediately before them and immediately after them will be selected as missed true positives (MTP). These MTP are thus added to the vectors \mathbf{U} and \mathbf{V} at their designated locations in the vectors. A segment of 25000 in Fig. 2.6 is used to

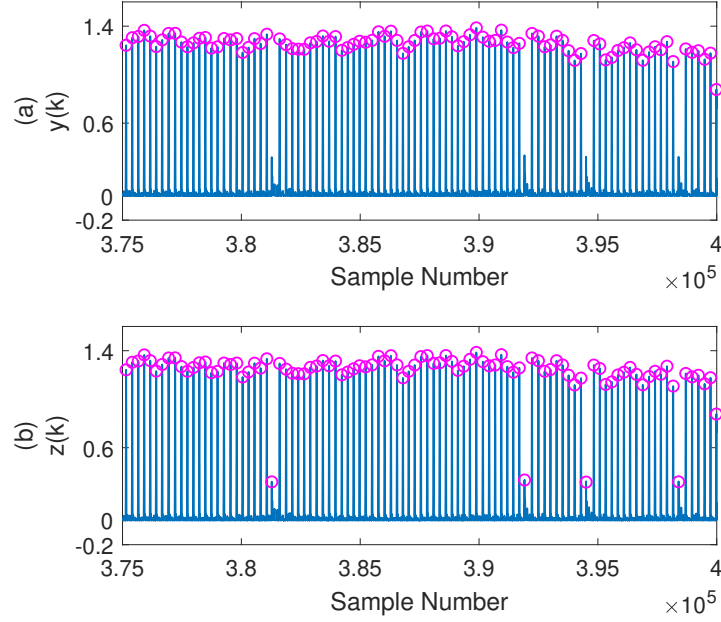


Figure 2.6: Search back in record 109 with y-axis in mV (1039-1108s) of MIT-BIH arrhythmia database. (a) Peaks detected after False peak elimination, (b) Low amplitude peaks detected resulting from search back.

display the results of using this stage. The segment is taken from record 109 where the peak amplitude is too low to be detected in the peak detection stage. Figure 2.6(a) shows the missed peaks in the segment while Fig. 2.6(b) shows the detected peaks resulting from the search back stage.

Thus, using step by step learning and statistical analysis of smaller segments, the method can detect the maximum numbers of true peaks.

2.4 Experiment and Results

The proposed method has been implemented in MATLAB R2020a 2.6 GHz Intel Core i7 CPU with 16 GB RAM and 64-bit Windows 10 operating system. As mentioned earlier the databases used were MIT-BIH arrhythmia and Fantasia databases with 48 records each with a duration of 30 minutes and 40 records each with a duration of 2 hours, respectively. To maintain peak detection logic a total of 142.5 seconds of data of record 207 from the MIT-BIH database is excluded that contains ventricular flutter. Three merits of evaluation are used to measure the overall performance of the proposed method, and these are sensitivity (Se), positive predictivity ($P+$), and

detection error rate (*DER*) which are represented by,

$$Se = \frac{TP}{TP + FN}, \quad (2.13)$$

$$P+ = \frac{TP}{TP + FP}, \quad (2.14)$$

$$DER = \frac{FP + FN}{TB}, \quad (2.15)$$

Where, *TP* is the true positive that is the number of annotated beats detected properly, *FN* is the false negatives that are the number of missed beats from the annotations, *FP* is the false positive that is the number of beats that are not annotated but still detected by the algorithm and *TB* is the total number of beats annotated in the record.

The proposed method is summarized by Algorithm 1 and the results are represented in Table 2.2 for MIT-BIH arrhythmia database and Table 2.3 for the Fantasia database. The results displayed in the paper are better compared to most of the previous methods and show better performance especially for records with changes in morphology. In both the tables, *DB* is the number of detected beats. The overall performance for the MIT-BIH database is classified to have a sensitivity (*Se*) of 99.82%, positive predictivity (*P+*) of 99.88%, and a very low detection error rate (*DER*) of 0.31%. It is important to state that it is more significant to minimize the number of false positives (*FP*) than the number of false negatives (*FN*). The reason behind this is that detecting false peaks gives the doctors ambiguous results and therefore wrong diagnosis while if a few peaks are missed then the heart rate reduces hence by observing the trend of the R-peaks, the doctors can predict where those peaks are located. Such peaks were missed due to their low amplitudes. The algorithm only faced problems with record 203 which is a difficult record even for physicians to detect [46]. This record contains morphological changes, multiform PVCs, and a high amount of instrumental noise like baseline wander, muscle movement noise, and noise from unknown sources. As for the rest of the records, the performance is high compared to any other method mentioned in this paper.

Table 2.2: Results from the MIT-BIH arrhythmia database.

Rec. No.	<i>TB</i>	<i>DB</i>	<i>TP</i>	<i>FP</i>	<i>FN</i>	<i>Se</i> (%)	<i>P+</i> (%)	<i>DER</i> (%)
100	2273	2273	2273	0	0	100.00	100.00	0.00
101	1865	1865	1865	0	0	100.00	100.00	0.00
102	2187	2187	2187	0	0	100.00	100.00	0.00

Rec. No.	<i>TB</i>	<i>DB</i>	<i>TP</i>	<i>FP</i>	<i>FN</i>	<i>Se(%)</i>	<i>P+(%)</i>	<i>DER(%)</i>
103	2084	2084	2083	1	1	99.95	99.95	0.10
104	2229	2230	2229	1	0	100.00	99.96	0.00
105	2572	2581	2565	16	7	99.73	99.38	0.89
106	2027	2014	2013	1	12	99.31	99.95	0.64
107	2137	2143	2137	6	0	100.00	99.72	0.28
108	1763	1763	1753	10	10	99.43	99.43	1.13
109	2532	2532	2532	0	0	100.00	100.00	0.00
111	2124	2126	2124	2	0	100.00	99.91	0.09
112	2539	2542	2539	3	0	100.00	99.88	0.12
113	1795	1795	1795	0	0	100.00	100.00	0.00
114	1879	1878	1878	0	1	99.95	100.00	0.05
115	1953	1953	1953	0	0	100.00	100.00	0.00
116	2412	2395	2393	2	19	99.21	99.92	0.87
117	1535	1537	1535	2	0	100.00	99.87	0.13
118	2278	2278	2278	0	0	100.00	100.00	0.00
119	1987	1988	1987	1	0	100.00	99.95	0.05
121	1863	1863	1862	1	1	99.95	99.95	0.11
122	2476	2476	2476	0	0	100.00	100.00	0.00
123	1518	1521	1518	3	0	100.00	99.80	0.20
124	1619	1619	1619	0	0	100.00	100.00	0.00
200	2601	2599	2599	0	2	99.92	100.00	0.08
201	1963	1960	1955	5	8	99.59	99.74	0.66
202	2136	2137	2131	6	5	99.77	99.72	0.51
203	2980	2933	2898	35	82	97.25	98.81	3.93
205	2656	2642	2642	0	14	99.47	100.00	0.53
207	1860	1869	1860	9	0	100.00	99.52	0.48
208	2955	2948	2945	3	10	99.66	99.90	0.44
209	3005	2999	2999	0	6	99.80	100.00	0.20
210	2650	2638	2638	0	12	99.55	100.00	0.45
212	2748	2751	2748	3	0	100.00	99.89	0.11
213	3251	3247	3247	0	4	99.88	100.00	0.12
214	2262	2265	2262	3	0	100.00	99.87	0.13
215	3363	3369	3363	6	0	100.00	99.82	0.18
217	2208	2208	2208	0	0	100.00	100.00	0.00
219	2154	2157	2154	3	0	100.00	99.86	0.14
220	2048	2050	2048	2	0	100.00	99.90	0.10

Rec. No.	<i>TB</i>	<i>DB</i>	<i>TP</i>	<i>FP</i>	<i>FN</i>	<i>Se(%)</i>	<i>P+(%)</i>	<i>DER(%)</i>
221	2427	2426	2426	0	1	99.96	100.00	0.04
222	2483	2485	2483	2	0	100.00	99.92	0.08
223	2605	2605	2604	1	1	99.96	99.96	0.08
228	2053	2056	2051	5	2	99.90	99.76	0.34
230	2256	2258	2256	2	0	100.00	99.91	0.09
231	1571	1571	1571	0	0	100.00	100.00	0.00
232	1780	1782	1780	2	0	100.00	99.89	0.11
233	3079	3077	3077	0	2	99.94	100.00	0.06
234	2753	2753	2753	0	0	100.00	100.00	0.00
Total	109494	109428	109292	136	200	99.82	99.88	0.31

Table 2.3: Results from Fantasia database

Rec. No.	<i>TB</i>	<i>DB</i>	<i>TP</i>	<i>FP</i>	<i>FN</i>	<i>Se(%)</i>	<i>P+(%)</i>	<i>DER(%)</i>
F1o01	7169	7172	7169	3	0	100.00	99.96	0.04
F1o02	6823	6811	6811	0	12	99.82	100.00	0.18
F1o03	7228	7230	7225	5	3	99.96	99.93	0.11
F1o04	6230	6251	6228	23	2	99.97	99.63	0.40
F1o05	5730	5737	5730	7	0	100.00	99.88	0.12
F1o06	6231	6233	6231	2	0	100.00	99.97	0.03
F1o07	7150	7134	7125	9	25	99.65	99.87	0.48
F1o08	8485	8485	8481	4	4	99.95	99.95	0.09
F1o09	4925	4930	4925	5	0	100.00	99.90	0.10
F1o10	8241	8241	8240	1	1	99.99	99.99	0.02
F1y01	8709	8711	8709	2	0	100.00	99.98	0.02
F1y02	7035	7039	7035	4	0	100.00	99.94	0.06
F1y03	7643	7647	7643	4	0	100.00	99.95	0.05
F1y04	5511	5511	5511	0	0	100.00	100.00	0.00
F1y05	6965	6968	6965	3	0	100.00	99.96	0.04
F1y06	7086	7088	7078	10	8	99.89	99.86	0.25
F1y07	5947	5950	5945	5	2	99.97	99.92	0.12
F1y08	7289	7291	7289	2	0	100.00	99.97	0.03
F1y09	8021	8020	8018	2	3	99.96	99.98	0.06
F1y10	8693	8693	8693	0	0	100.00	100.00	0.00
F2o01	7234	7236	7231	5	3	99.96	99.93	0.11
F2o02	6372	6368	6364	4	8	99.87	99.94	0.19

Rec. No.	<i>TB</i>	<i>DB</i>	<i>TP</i>	<i>FP</i>	<i>FN</i>	<i>Se</i>(%)	<i>P+</i>(%)	<i>DER</i>(%)
F2o03	6541	6540	6537	3	4	99.94	99.95	0.11
F2o04	6902	6902	6901	1	1	99.99	99.99	0.03
F2o05	8469	8486	8466	20	3	99.96	99.76	0.27
F2o06	5249	5249	5249	0	0	100.00	100.00	0.00
F2o07	5944	5944	5944	0	0	100.00	100.00	0.00
F2o08	7044	7095	6984	111	60	99.15	98.44	2.43
F2o09	6138	6139	6137	2	1	99.98	99.97	0.05
F2o10	8441	8439	8429	10	12	99.86	99.88	0.26
F2y01	8106	8107	8104	3	2	99.98	99.96	0.06
F2y02	6574	6573	6573	0	1	99.98	100.00	0.02
F2y03	6807	6810	6807	3	0	100.00	99.96	0.04
F2y04	8603	8604	8604	0	0	100.01	100.00	0.00
F2y05	9244	9239	9236	3	8	99.91	99.97	0.12
F2y06	6851	6853	6851	2	0	100.00	99.97	0.03
F2y07	6506	6506	6506	0	0	100.00	100.00	0.00
F2y08	7358	7343	7329	14	29	99.61	99.81	0.58
F2y09	8701	8697	8685	12	16	99.82	99.86	0.32
F2y10	7113	7097	7093	0	16	99.72	99.94	0.22
Total	285308	285369	285081	284	224	99.92	99.90	0.18

The Fantasia database shows even better performance for all records even for records with low sound to noise ratio (SNR). As for the rest of the records it works well giving higher accuracy. The overall performance for the proposed algorithm on this database is classified to have a sensitivity (*Se*) of 99.92%, positive predictivity (*P+*) of 99.90%, and an even lower detection error rate (*DER*) of 0.18%.

The average time taken to run the algorithm on 30 minutes of a record is 3.5 seconds. Figures 2.7-2.10 represent what roles different stages in the proposed algorithm play in detecting QRS complexes in various scenarios. A noisy segment of each of these records is displayed in these figures and along with the detection of peaks in the original signal. In Fig. 2.7 there are low amounts of noise with the baseline shift, which is fixed, and the peaks are detected properly. Figure 2.8 shows the PVCs which are there in the place of R-peaks and they are properly detected even with P and T waves surrounding them. Figure 2.9 shows a segment of record 104 with high-frequency EMG contaminating it. The noise is not completely filtered out, but the R-peaks are detected without any false negatives or positives. Lastly, Fig. 2.10 shows a segment of

Algorithm 1 The proposed algorithm.

- 1: **Initials** $K, j, \mathbf{W}, \mathbf{w}, \mathbf{Z}_t$
 - 2: Read K samples of the input ECG signal $x(k)$
 - 3: Preprocessing using denoising filters (median filters, moving average filter), as in Section 2.3.1
 - 4: Divide $x_3(k)$ into R number of segments of j samples
 - 5: Find the fiducial mark, $d(k)$, as in Section 2.3.2
 - 6: Let $i = 1$
 - 7: **while** $i < R$
 - 8: Input segment number i of $d(k)$
 - 9: Compute A , by using (2.1)
 - 10: Compute C , as in Section 2.3.2
 - 11: Process segment number i of $d(k)$ with amplitude threshold C and 320 ms minimum peak-to-peak interval
 - 12: Compute D , by using (2.2)
 - 13: Compute G , by using (2.3)
 - 14: Eliminate false peaks to obtain \mathbf{w} , by using (2.4)
 - 15: $\mathbf{W} = [\mathbf{W} \quad \mathbf{w}]$
 - 16: $i = i + 1$
 - 17: **End**
 - 18: Compute H , by using (2.6)
 - 19: Process \mathbf{W} with H to eliminate overlapped peaks to get $y(n)$
 - 20: Let $i = 1$
 - 21: Divide $y(n)$ into R number of segments of j samples each
 - 22: **while** $i < R$
 - 23: Compute B , by using (2.7)
 - 24: Compute Z , by using (2.8)
 - 25: Compute S , by using (2.9)
 - 26: Compute Y , by using (2.10)
 - 27: Compute X , by using (2.11)
 - 28: Compute M , by using (2.12)
 - 29: **if** $S \leq 100$ samples
 - 30: Process segment number i of $y(n)$ with amplitude threshold B and Y samples maximum peak-to-peak interval
 - 31: **if** any peak-to-peak interval in $y(n) > Y$
 - find peaks in that interval with minimum peak-to-peak interval X and minimum amplitude threshold of B and store it in vector \mathbf{a}
 - Select only the peaks that are more than M samples away from the the true peak preceding it and the true peak after it
-

```

32:   End
33:   End
34:    $\mathbf{Z}_t = [\mathbf{Z}_t \quad \mathbf{a}]$ 
35:    $i = i + 1$ 
36: End
37: Return  $\mathbf{Z}_t$ 

```

record 203 which contains both high-frequency and low-frequency noises along with multiform PVCs. Therefore, not all peaks are detected correctly, and this results in some false positives and negatives. The pink circles show the detected peaks on the preprocessed signal, $x_3(k)$, while the red circles display the peaks detected on the median filtered signal $x_2(k)$. The locations of the peaks on the raw ECG signal, $x(k)$ are shown by using red circles for each figure.

2.5 Comparison with the State-of-the-Art Methods

The proposed method is compared to several the-state-of-the-art techniques on different databases. The results of the comparison for MIT-BIH arrhythmia database is shown in Table 2.4. It contains eleven other methods over a vast timeline with eight of these methods being fairly recent in the field. It is seen that the proposed algorithm has superior performance in detecting QRS over all other methods in all aspects except for three, which are A. Sharma *et al.* [25], T. Sharma *et al.* [13], and L. Bouny *et al.* [24].

Table 2.4: Comparison with state-of-the-art methods

Reference	Year	TB	TP	FP	FN	$P+(\%)$	$Se(\%)$	$DER(\%)$
Pan et al. [7]	1985	116137	115860	507	277	99.56	99.76	0.68
Hamilton et al. [8]	1986	109267	108927	248	340	99.77	99.69	0.54
Christov [38]	2004	110050	109615	239	240	99.65	99.74	0.44
Zidelmal et al. [22]	2012	109494	109101	193	393	99.82	99.64	0.54
Pandit et al. [39]	2017	109809	109432	369	389	99.66	99.65	0.69
Sharma et al. [13]	2017	109494	109381	136	113	99.88	99.90	0.23
Tang et al. [45]	2018	109966	109055	494	911	99.55	99.17	1.28
Sharma et al. [25]	2019	109494	109363	131	183	99.83	99.89	0.29
Zalabarria et al. [36]	2020	106581	106096	431	485	99.60	99.54	0.86
Bouny et al. [24]	2020	109494	109316	147	178	99.87	99.84	0.30
Zhang et al. [48]	2020	109966	109124	683	842	99.38	99.23	1.39
Proposed Method	2020	109494	109293	136	200	99.88	99.82	0.31

Thus, those methods are further compared to the proposed algorithm. Table 2.5 rep-

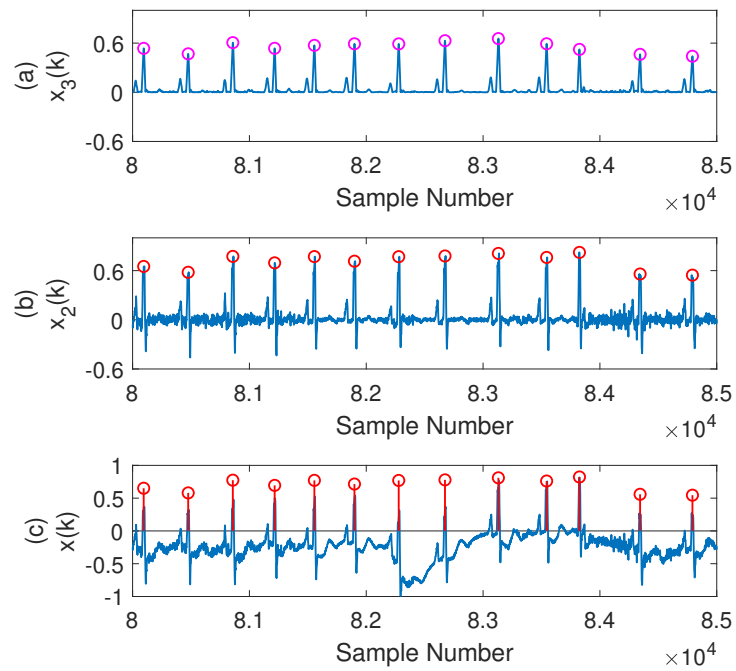


Figure 2.7: Outputs obtained from record 108 with y-axis in mV (222-236s). (a) Peak detected on preprocessed signal, where the pink circles provided show the detected peaks on $x_3(k)$. (b) Peaks detected on the baseline corrected signal where the red circles show the detected peaks on $x_2(k)$. (c) Peaks detected on the original signal where the red circles show the locations of the peaks in $x(k)$.

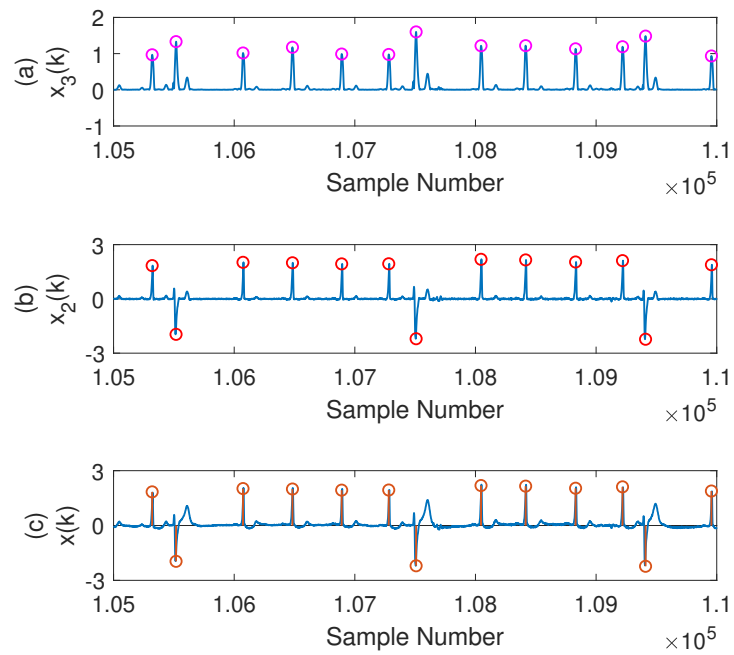


Figure 2.8: Outputs obtained from record 114 with y-axis in mV (291-305s). (a) Peak detected on preprocessed signal, where the pink circles provided show the detected peaks on $x_3(k)$, (b) Peaks detected on the baseline corrected signal where the red circles show the detected peaks on $x_2(k)$, (c) Peaks detected on the original signal where the red circles show the locations of the peaks in $x(k)$.

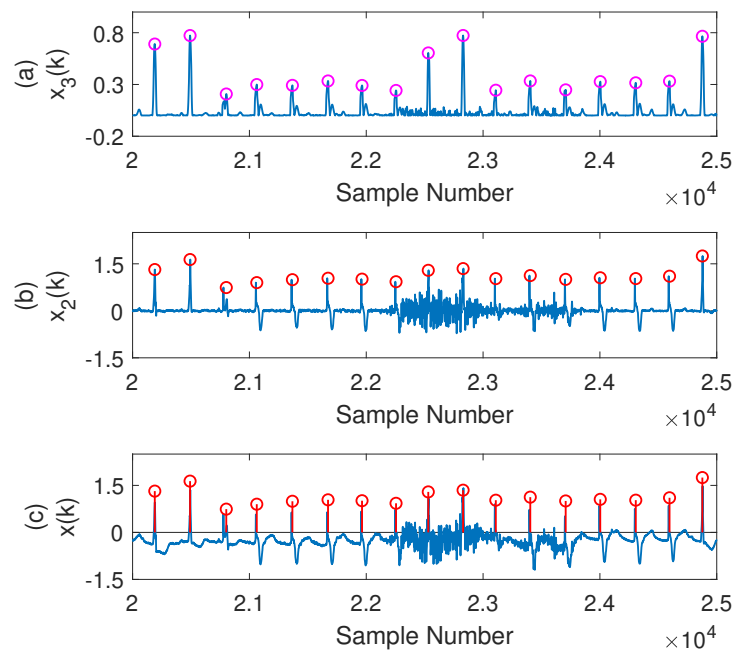


Figure 2.9: Outputs obtained from record 104 with y-axis in mV (56-70s). (a) Peak detected on preprocessed signal, where the pink circles provided show the detected peaks on $x_3(k)$, (b) Peaks detected on the baseline corrected signal where the red circles show the detected peaks on $x_2(k)$, (c) Peaks detected on the original signal where the red circles show the locations of the peaks in $x(k)$.

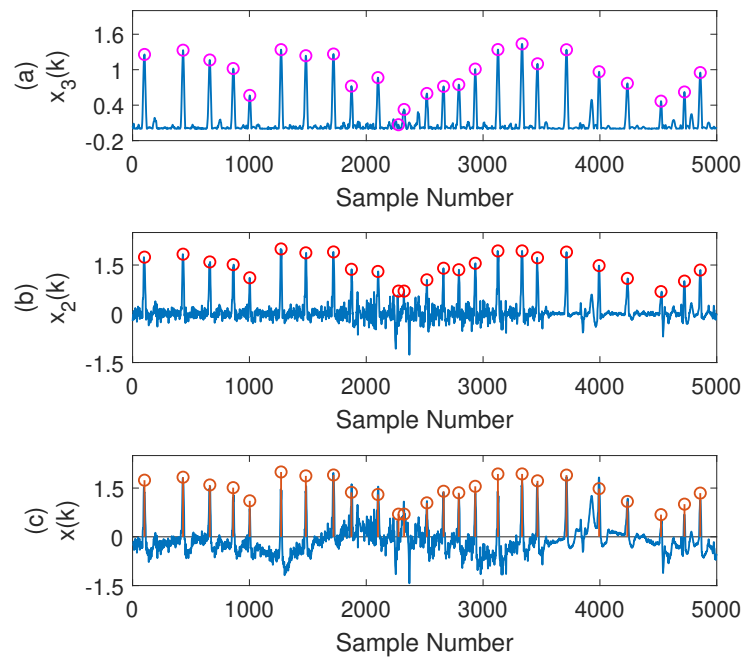


Figure 2.10: Outputs obtained from record 203 with y-axis in mV (0-14s). (a) Peak detected on preprocessed signal, where the pink circles provided show the detected peaks on $x_3(k)$, (b) Peaks detected on the baseline corrected signal where the red circles show the detected peaks on $x_2(k)$, (c) Peaks detected on the original signal where the red circles show the locations of the peaks in $x(k)$.

resents a detailed comparison between these three methods and ours on noisy signals from the MIT-BIH database. The records selected are 104, 105, 108, 113, 201, 203, 205, 207, 208, 210, 228, and 232 according to [24]. These records contain either substantial noise or high amplitude P and T waves and so they are ideal for comparison. It is seen that out of the 12 records considered, the proposed method has overall better performance on 5 occasions which are records 104, 113, 208, 228 and 232, than any of the other three methods. In addition to that, the proposed method also shows better sensitivity for record 207 and positive predictivity for records 105, 108, 205, and 210 than any other. However, T. Sharma *et al.* [13] shows better detection than all the algorithms including the proposed method on three occasions which are 108, 201, and 207 for both sensitivity and positive predictivity while A. Sharma *et al.* [25] shows better detection in only one occasion which is for record 205. The method of L. Bouny *et al.* [24] clearly does not show a better overall performance than the proposed method. The method shows better sensitivity on five occasions, however, the positive predictivity and detection error rate suffers and in most cases is lower than the proposed algorithm. The method of A. Sharma *et al.* [25] also shows better sensitivity than the proposed method on five occasions out of twelve, however, similar to L. Bouny *et al.* [24], the method has lower positive predictivity and detection error rate for ten out of twelve records than the proposed method. The method in T. Sharma *et al.* [13] shows better sensitivity on six records, better positive predictivity on three records, and lower detection error rate on five records compared to the proposed algorithm. As a result, it can be stated that the proposed algorithm has higher overall positive predictivity than all three of the methods. The record 203 shows the least performance for the proposed method as it is a highly fluctuating record with high amounts of noise, multiform PVCs and random morphological changes. Seeing these statistics, it could easily be said that even if the proposed method has an overall better performance than those of A. Sharma *et al.* [25] and L. Bouny *et al.* [24] but it is still inferior to the method of T. Sharma *et al.* [13] in terms of sensitivity. Therefore, this method is selected for further comparison using Fantasia and European ST-T databases.

Twenty records from each database are selected according to [13] and each record is clipped to one million samples for a fair comparison. Table 2.6 presents the comparison results. It is seen that, in most cases, the proposed algorithm performs far better than that in [13] and produces far lower false positives. Even though the method of T. Sharma *et al.* [13] shows better accuracy for sensitivity in the European ST-T database, nevertheless, that method does not perform well in noisy conditions. The sensitivity of the proposed algorithm is slightly lower than that of the method of T.

Table 2.5: Comparison of noisy records with three state-of-the-art methods

	A. Sharma et al. [25]			T. Sharma et al. [13]			L. Bouny et al. [24]			Proposed Method		
Rec. No.	Se(%)	P+(%)	DER(%)	Se(%)	P+(%)	DER(%)	Se(%)	P+(%)	DER(%)	Se(%)	P+(%)	DER(%)
104	99.6	99.15	1.26	99.69	99.64	0.68	99.78	99.51	0.72	100	99.95	0.05
105	99.81	99	1.21	99.42	98.76	1.84	99.22	98.53	2.26	99.73	99.38	0.89
108	99.32	99.09	1.59	99.6	99.43	0.97	99.55	98.98	1.48	99.43	99.43	1.13
113	99.94	99.89	0.17	100	100	0	100	100	0	100	100	0
201	99.85	100	0.15	99.95	100	0.05	99.64	99.54	0.82	99.59	99.74	0.66
203	99.19	99.5	1.31	98.99	99.59	1.42	98.76	99.49	1.75	97.25	98.81	3.93
205	99.96	100	0.04	99.89	100	0.11	99.89	100	0.11	99.47	100	0.53
207	99.68	98.67	1.67	100	99.79	0.22	99.95	99.57	0.48	100	99.52	0.48
208	99.29	99.63	1.08	99.42	99.80	0.78	99.32	99.83	0.85	99.66	99.90	0.44
210	99.81	99.92	0.26	99.96	99.89	0.15	99.66	99.92	0.41	99.55	100	0.45
228	99.85	98.99	1.17	99.95	98.94	1.12	99.66	99.47	0.88	99.9	99.76	0.34
232	100	99.83	0.17	100	99.55	0.45	100	99.78	0.23	100	99.89	0.11

Table 2.6: Comparison with T. Sharma et al. [13] on two databases

European ST Database														
Fantasia Database						Sharma et al. [13]								
	Rec	Se(%)	P+(%)	DER(%)	Proposed Algorithm	Rec	Se(%)	P+(%)	DER(%)	Sharma et al. [13]	Proposed Algorithm			
	F1o01	99	99.55	1.47	100.00	99.96	0.04	e0103	99.88	98.66	1.48	99.41	99.80	0.79
	F1o02	100	98.1	1.94	99.82	100.00	0.18	e0105	99.97	99.95	0.08	99.54	99.76	0.70
	F1o03	100	98.78	1.24	99.96	99.93	0.11	e0107	99.97	99.82	0.2	99.87	99.92	0.20
	F1o05	99.91	99.53	0.56	100.00	99.88	0.12	e0112	99.97	97.33	2.78	99.60	99.70	0.70
	F1o07	100	99.68	0.32	99.65	99.87	0.48	e0121	99.89	99.7	0.42	99.87	99.85	0.28
	F1y01	100	99.76	0.24	100.00	99.98	0.02	e0127	99.67	99.33	1.01	100.00	99.98	0.02
	F1y07	100	99.79	0.21	99.97	99.92	0.12	e0133	99.95	99.57	0.49	99.84	99.95	0.22
	F1y08	99.98	99.44	0.59	100.00	99.97	0.03	e0136	100	100	0	100.00	100.00	0.00
	F1y09	100	99.73	0.27	99.96	99.98	0.06	e0147	100	99.97	0.03	99.97	100.00	0.03
	F1y10	100	99.76	0.24	100.00	100.00	0.00	e0154	100	99.7	0.31	99.57	99.95	0.48
	F2o01	100	100	0	99.96	99.93	0.11	e0202	99.75	99.96	0.29	99.32	99.96	0.68
	F2o02	99.92	99.94	0.14	99.87	99.94	0.19	e0205	98.71	99.98	1.32	99.54	98.97	1.50
	F2o03	100	99.29	0.72	99.94	99.95	0.11	e0208	99.75	99.77	0.48	99.84	99.96	0.21
	F2o04	100	100	0	99.99	99.99	0.03	e0213	99.26	99.88	0.86	98.90	99.75	1.35
	F2o05	99.86	99.92	0.22	99.96	99.76	0.27	e0303	99.9	99.9	0.21	99.92	99.98	0.10
	F2y01	100	99.7	0.31	99.98	99.96	0.06	e0403	99.94	99.94	0.12	100.00	99.69	0.31
	F2y02	100	99.93	0.07	99.98	100.00	0.02	e0411	99.94	99.98	0.07	99.72	99.94	0.34
	F2y03	99.97	99.33	0.7	100.00	99.96	0.04	e0418	100	100	0	100.00	99.98	0.02
	F2y04	99.96	99.64	0.41	100.00	100.00	0.00	e0509	100	99.98	0.02	99.56	99.98	0.46
	F2y05	99.57	99.92	0.5	99.91	99.97	0.12	e0612	99.89	99.12	1	100.00	100.00	0.00
Total	99.95	99.73	0.32	0.10	99.95	99.95	0.10	Total	99.82	99.63	0.56	99.72	99.84	0.45

Sharma *et al.* [13], while the positive predictivity of the proposed algorithm is higher than that of [13]. The proposed method also shows a lower detection error rate using both databases which mean more accuracy of true detection. Therefore, it can be verified that the proposed algorithm presents an overall better performance on the average than the method in [13] and can better adapt to the changes in the morphology of the ECG signal. The reason behind this is that the proposed algorithm does not contain any non-linear transformations and is the statistical detection of ECG records with two-dimensional thresholds.

2.6 Conclusion

In this chapter, a novel method of QRS detection using a simple statistical analysis of the ECG has been presented. Median filtering, moving average filtering, segmentation, false peak elimination, and search back has been considered in this paper for effective detection of QRS complexes. The number of segments chosen for each record has been varied automatically over the course of two distinct databases. It has been seen that the use of median filters could minimize the P and T waves, and the baseline wander. Dividing the record into multiple segments resulted in low processing time and better accuracy. Furthermore, statistically eliminating false peaks, identified very few false positives and therefore have shown better positive predictivity than any other methods mentioned in the paper. Similarly, the search back stage was able to identify missing low amplitude peaks by considering the standard deviations of each segment in a record. Simulation results have shown better performance in most of the records than other state-of-the-art methods. Thus, the proposed algorithm performs better in terms of automatic detection with a higher percentage of overall detection rate.

Chapter 3

Single Channel QRS Detection Using Discrete Wavelet Transform And Median Denoising With Adaptive Multilevel Thresholding

3.1 Introduction

In this chapter, we present a new method of peak detection in ECG using adaptive multilevel thresholding. The amplitudes of the noise and P and T waves are often smaller compared to R-peaks. However, the amplitudes of R-peaks vary through any ECG record due to different types of anomalies in the heart. The heart rates might increase or decrease in amplitude at times when a person experiences arrhythmia and so one particular amplitude threshold is not able to detect beats properly no matter how much the noise is reduced. Therefore, any amplitude threshold put in place to separate the R-peaks and ectopic beats from the noise peaks must be varied. The notion of automatic detection relies on thresholds that can be varied automatically without human intervention. Furthermore, one level of adaptive thresholding is not effective to distinguish between peaks. Thus, the proposed method that utilizes two levels of adaptive amplitude threshold. Two levels of beat rate thresholds are also used to process the ECG signals in the MIT-BIH database [51] containing 48 records of patients with arrhythmias. The method works well with most records and produces an overall sensitivity (Se) of 99.74%, a positive predictivity ($P+$) of 99.88%, and a detection error rate (DER) of only 0.38%. The method is highly robust in adapting to the morphological changes in ECG signals.

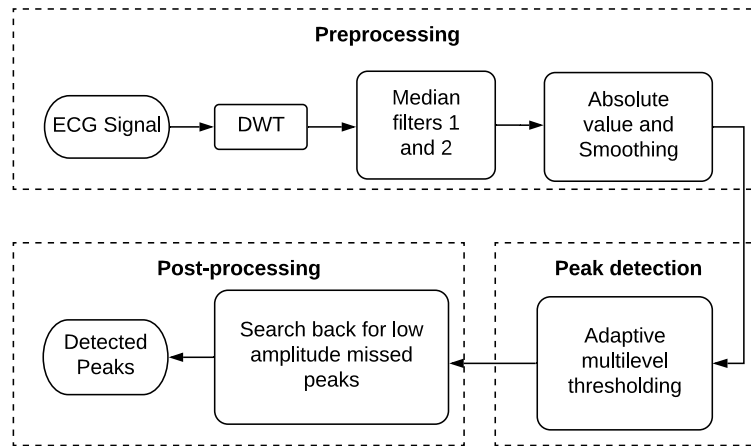


Figure 3.1: Block diagram for the proposed method.

3.2 The Proposed Method

Figure 3.1 shows the block diagram of the proposed method. The diagram contains three stages, namely, a preprocessing stage to remove or minimize noise, a peak detection stage that passes the preprocessed ECG signal through one hard threshold and three distinct adaptive thresholds to detect the R-peaks and the premature ventricular contractions (PVCs), and finally a post-processing stage to detect any peaks that were missed in the initial detection because of their low amplitudes. Results from the individual stages are illustrated based on applying data from MIT-BIH arrhythmia database [51].

3.2.1 Preprocessing

The preprocessing stage consists of three steps, first, discrete wavelet transform (DWT) is used with three levels of decomposition and only the approximate signal of the third level is selected to reconstruct the signal. The second step has two median filters to eliminate the baseline wander which is a low-frequency artifact. This also reduces the peak amplitude of the P and T waves and so makes the peak detection stage simpler. The third step is to find the absolute value of the signal and then smoothing it to produce an envelope.

Discrete Wavelet Transform (DWT)

Figure 3.2 illustrates the DWT to three levels for a better understanding of the preprocessing procedure. In this work, the signal is first decomposed using DWT to three levels. DWT is a linear transformation of non-stationary signals [15]. It is a tool

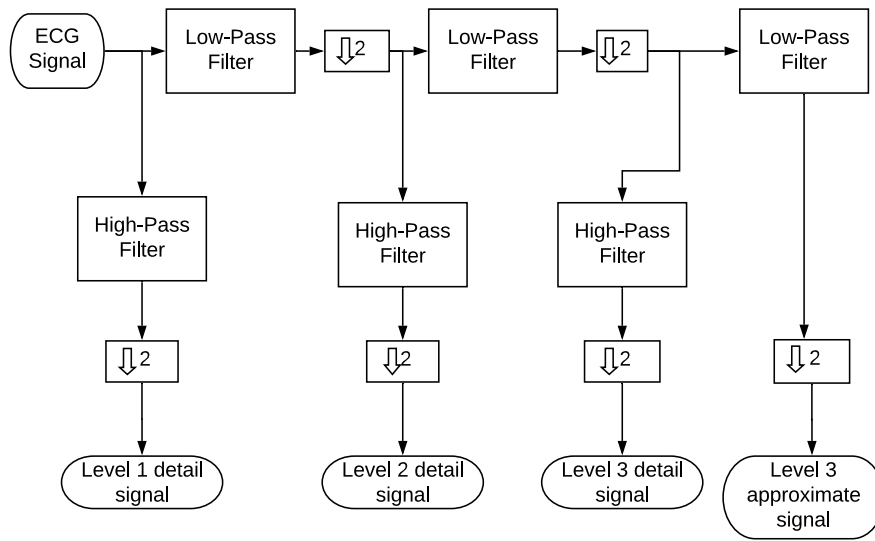


Figure 3.2: Wavelet decomposition to three levels.

that can recognize sharp changes in the input signal depending on the mother wavelet used to analyze the signal [15]. DWT is performed using filter banks to decompose the signal into different frequency subbands and then again reconstructing the signal. Each level uses a filter bank consisting of a high-pass and a low pass filter followed by decimation by 2 for both filters. The signal obtained from the high pass filter is called the detail signal and from the low pass filter is called the approximate signal [7]. This goes on for three levels in the octave band structure. Each time the frequency is divided by a factor of 2. For the MIT-BIH arrhythmia database [51, 53], the sampling frequency is 360 Hz and so the frequency ranges of detail signal lie between 90-180 Hz, 45-90 Hz, 0-45 Hz, for stages one, two, and three, respectively. It is clear from [7] that the majority of the information on the ECG signal falls between 5 Hz and 15 Hz, however, according to [6], some vital information of the ECG signal can be found till 35 Hz frequency range. Therefore, for the proposed technique, the approximate signal for level three that is in the frequency range of 0 to 45 Hz are selected to reconstruct the signal. The reason for this is that the algorithm tries to capture as much information of the QRS complex as possible. Figure 3.3 shows the different stages of the wavelet decomposition. The wavelet used in this study is the *coif2* wavelet which is a near symmetric orthogonal wavelet available as a built-in function in MATLAB.

Median Filtering and Smoothing

After DWT, two median filters are used. The window sizes for the first and second filters are selected to be 100 ms, and 200 ms, respectively. The median filters in cas-

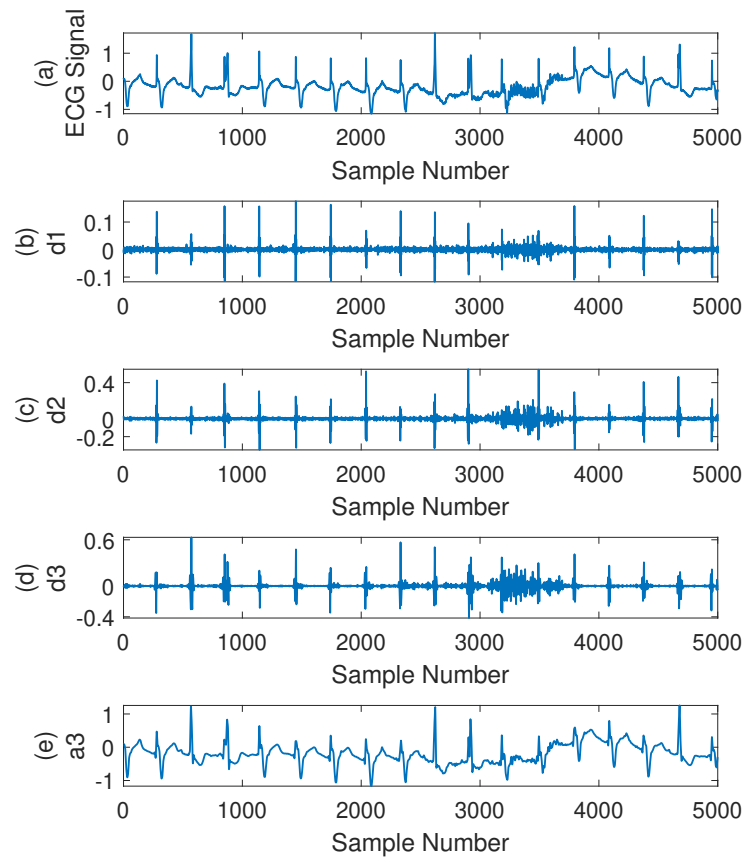


Figure 3.3: Wavelet transformed signals for scale level (1-3) for a section record 104 from the MIT-BIH arrhythmia database. (a) Raw ECG signal, (b) Detail signal for level 1, (c) Detail signal for level 2, (d) Detail signal for level 3, (e) Approximate signal for level 3.

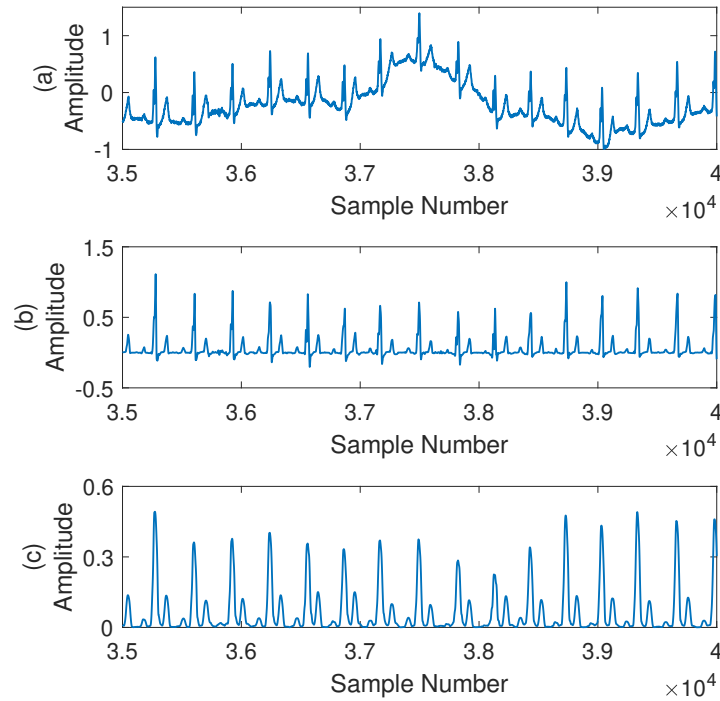


Figure 3.4: Outputs obtained from different stages with y-axis in mV. (a) ECG signal from record 111 of MIT-BIH database, (b) Signal obtained after median filtering, (c) Envelope obtained after smoothing.

ade can not only eliminate the baseline wander but also minimize the amplitudes of the P and T waves [19]. P waves occur approximately 50 ms before the QRS complex and T waves occur approximately 50 ms after the QRS complex and so 50 and 100 ms windows are selected to be implemented. To illustrate this effect, Fig. 3.4(a) shows the original ECG signal from records 111 of the MIT-BIH arrhythmia database with noise and Fig. 3.4(b) shows the effects of median filtering. After median filtering is performed the absolute value of the output from the median filters is obtained and a moving average window of 100 ms is considered to smooth the signal. This produces an envelope of the ECG signal and suppresses any high-frequency noise as well as EMG interference attained in the frequency range of 20 to 45 Hz. Figure 3.4(c) shows the envelope generated using this technique.

3.2.2 Peak detection using adaptive multilevel thresholding

After the preprocessing stage is complete, the peak detection stage starts with finding all the local peaks in the record with a peak-to-peak interval of 320 ms between adjacent peaks. The reason is that a beat rate over 200 beats/min is regarded as ventricular

flutter [55], approximately 190 beats/min or 3.15 beats/s is set as the beat rate threshold in order to maximize the number of detected true peaks.

Once all the local peaks are found, their amplitudes and locations are stored in vector \mathbf{P} and \mathbf{L} , respectively. We have used upper case boldface to denote the vectors. Here, the vectors \mathbf{P} and \mathbf{L} are given by, $\mathbf{P} = [P(1), P(2), P(3), \dots, P(N)]$ and $\mathbf{L} = [L(1), L(2), L(3), \dots, L(N)]$, where N is the total number of local peaks. The average value of the amplitudes of all these peaks in \mathbf{P} , denoted by T , is calculated as,

$$T = \frac{\sum_{n=1}^N P(n)}{N}, \quad (3.1)$$

where n is the position of the peak in vector \mathbf{P} .

Here, the adaptive multilevel thresholding (AMT) is applied. Two distinct levels of the signal, signal value (V_{sl}) and noise value (V_{nl}) are initialized to be 0. These values are used to update the thresholds with each selected true peak or discarded noise peak. Three initial thresholds, S , M , and R , are set to obtain the peaks, which are as,

$$S = 1.2T, \quad (3.2)$$

$$M = T, \quad (3.3)$$

$$R = 0.6T. \quad (3.4)$$

Here, R is regarded as the lower adaptive amplitude threshold below which all peaks are regarded as noise peaks and eliminated. The upper adaptive threshold, M , is used to eliminate peaks due to high-frequency noise and P and T waves. S is the non-adaptive amplitude threshold. Any peak amplitude in vector \mathbf{P} that exceeds S will be regarded as a true peak. The signal value for the true peaks detected using this threshold is updated using,,

$$V_{sl} = 0.05a + 0.95V_{sl}, \quad (3.5)$$

where a is the amplitude of the true peak. The algorithm also stores the detected true peaks in vectors \mathbf{G} and \mathbf{H} as true peak amplitudes and true peak locations, respectively. Here, the vectors, \mathbf{G} and \mathbf{H} are given by, $\mathbf{G} = [G(1), G(2), G(3), \dots, G(Q)]$ and $\mathbf{H} = [H(1), H(2), H(3), \dots, H(Q)]$, where Q is the total number of true peaks. The beat

rate of each true peak is calculated as,

$$B(i) = \frac{60f_s}{H(i+1) - H(i)}, \quad (3.6)$$

where i is the instantaneous position of the beat rate in vector \mathbf{B} and f_s is the sampling frequency of the ECG signal. If the peak value is less than threshold S but greater than threshold M , then $B(i)$ is checked against the beat rate threshold B_w , where B_w is given by,

$$B_w = \frac{2 \sum_{i=1}^{Q-1} B(i)}{Q-1}. \quad (3.7)$$

If $B(i)$ is found to be less than B_w then this peak is regarded as a true peak and its peak amplitude and location will be added to \mathbf{G} and \mathbf{H} , respectively. The signal value is then updated as,

$$V_{sl} = 0.1a + 0.9V_{sl}. \quad (3.8)$$

However, if this is not the case and $B(i)$ is greater than B_w , then the peak is regarded as a noise peak and is discarded and the noise value is updated by,

$$V_{nl} = 0.2a + 0.8V_{nl}. \quad (3.9)$$

Finally, if any peak is still lesser than threshold M but greater than threshold R , then, $B(i)$ is checked against B_z , where, B_z is given by,

$$B_z = \frac{1.25 \sum_{i=1}^{Q-1} B(i)}{Q-1}. \quad (3.10)$$

If $B(i)$ is less than the beat rate threshold B_z then the peak is regarded as a true peak and its peak amplitude and location will be added to \mathbf{G} and \mathbf{H} respectively. The signal level is again updated using (3.8). However, if $B(i)$ is greater than B_z then the peak will again be removed as it is considered as a noise peak and the noise level will be updated using (3.9). After classifying the peak as a true peak or a noise peak the threshold M is updated as,

$$M = 0.8V_{nl} + 0.25(0.8V_{sl} - V_{nl}), \quad (3.11)$$

and the threshold R is updated as,

$$R = 0.5M. \quad (3.12)$$

Once, the thresholds are updated the entire process will be repeated for the next peak and the thresholds will be updated. In this way, the thresholds are varied so can adapt to sudden changes in the amplitude of the record resulting in high accuracy.

3.2.3 Post-processing

The aim of this stage is to search for low amplitude missed peaks by taking the peak-to-peak intervals for the detected peak into consideration. Once all the peaks are found and stored in vector \mathbf{H} , the peak-to-peak intervals are calculated and stored in vector \mathbf{K} , as,

$$K(i) = H(i+1) - H(i), \quad (3.13)$$

where i is the instantaneous position of the peaks in \mathbf{G} and \mathbf{H} .

Here, $\mathbf{K} = [K(1), K(2), K(3), \dots, K(Q-1)]$. An x-axis threshold for the maximum peak-to-peak interval allowed between adjacent peaks will be calculated as,

$$F = \frac{2 \sum_{i=1}^{Q-1} K(i)}{Q-1}. \quad (3.14)$$

If it is found that the interval between any two adjacent peaks exceeds the value of F then the search back will be triggered and it will search for peaks within that interval between the corresponding peaks by lowering the amplitude threshold to 20% of M and peak-to-peak interval to 80% the value of F . Any peaks obtained through this method are regarded as a low amplitude missed peaks and is added to the vectors \mathbf{G} and \mathbf{H} at their corresponding positions as true peaks. The process is repeated for the entire record to ensure maximum accuracy in detection.

3.3 Experiment and Results

The MIT-BIH arrhythmia database with 48 records, each with a duration of 30 minutes, are used in this experiment. Only channel MLII is used for the experiment and a total of 142.5 seconds of data from record 207 is excluded because it contains ventricular flutter. The evaluation of the proposed method uses the same figure of merits from Chapter 2, which are sensitivity (Se), positive predictivity ($P+$), and detection error rate (DER). These quantities are repeated here for clarity and they are represented by,

$$Se = \frac{TP}{TP + FN}, \quad (3.15)$$

$$P+ = \frac{TP}{TP + FP}, \quad (3.16)$$

$$DER = \frac{FP + FN}{TB}, \quad (3.17)$$

where, TP is the number of true positives, FN is the number of false negatives, FP is the number of false positives and TB is the total number of beats annotated in the record. The proposed method is summarized by Algorithm 2. Table 3.1 represents the results of running 48 records from the MIT-BIH arrhythmia database. Here, DB is the number of detected beats. The results obtained show a high sensitivity of 99.74%, a positive predictivity of 99.88%, and a detection error rate of only 0.38%. The proposed method is further compared to four other state-of-the-art methods and shows better accuracy in all aspects than three of them. This is represented in Table 3.2. Even if the method of Pan *et al.*[7] shows higher sensitivity than the proposed algorithm, the recorded difference is negligible.. The positive predictivity for the proposed method is far better and gives a lower detection error rate than Pan *et al.* [7]. Figure 3.5(a) shows a section from record 108 of the MIT-BIH arrhythmia database. While, Fig. 3.5(b) represents the median filtered signal, and Fig. 3.5(c) represents the peak detection on the envelope obtained after smoothing. As shown in the figure, the upper and lower thresholds shown in red and black lines, respectively, experience change in values. The reason is that these two thresholds are varied adaptively and automatically over the course of the record and so they are subjected to change. The non-adaptive threshold is represented by the green line and does not change with the change in the signal to prevent the lower thresholds from exhibiting sharp sudden changes.

Table 3.1: Results from the MIT-BIH arrhythmia database

Rec. No.	TB	TP	FP	FN	$Se(\%)$	$P+(\%)$	$DER(\%)$
100	2273	2273	0	0	100.00	100.00	0.00
101	1865	1863	1	2	99.89	99.95	0.16
102	2187	2186	2	1	99.95	99.91	0.14
103	2084	2084	0	0	100.00	100.00	0.00
104	2229	2228	3	1	99.96	99.87	0.18
105	2572	2563	10	9	99.65	99.61	0.74
106	2027	2017	8	10	99.51	99.60	0.89
107	2137	2104	5	33	98.46	99.76	1.78
108	1763	1748	11	15	99.15	99.37	1.47
109	2532	2529	0	3	99.88	100.00	0.12
111	2124	2124	1	0	100.00	99.95	0.05

Rec. No.	<i>TB</i>	<i>TP</i>	<i>FP</i>	<i>FN</i>	<i>Se(%)</i>	<i>P+(%)</i>	<i>DER(%)</i>
112	2539	2539	1	0	100.00	99.96	0.04
113	1795	1795	0	0	100.00	100.00	0.00
114	1879	1878	0	1	99.95	100.00	0.05
115	1953	1953	0	0	100.00	100.00	0.00
116	2412	2394	1	18	99.25	99.96	0.79
117	1535	1535	0	0	100.00	100.00	0.00
118	2278	2278	0	0	100.00	100.00	0.00
119	1987	1987	1	0	100.00	99.95	0.05
121	1863	1861	1	2	99.89	99.95	0.16
122	2476	2476	0	0	100.00	100.00	0.00
123	1518	1518	0	0	100.00	100.00	0.00
124	1619	1618	0	1	99.94	100.00	0.06
200	2601	2589	11	12	99.54	99.58	0.88
201	1963	1955	2	8	99.59	99.90	0.51
202	2136	2129	2	7	99.67	99.91	0.42
203	2980	2898	19	82	97.25	99.35	3.39
205	2656	2636	6	20	99.25	99.77	0.98
207	1860	1858	13	2	99.89	99.31	0.81
208	2955	2946	1	9	99.70	99.97	0.34
209	3005	3005	2	0	100.00	99.93	0.07
210	2650	2619	5	31	98.83	99.81	1.36
212	2748	2748	0	0	100.00	100.00	0.00
213	3251	3239	3	12	99.63	99.91	0.46
214	2262	2262	0	0	100.00	100.00	0.00
215	3363	3361	1	2	99.94	99.97	0.09
217	2208	2207	0	1	99.95	100.00	0.05
219	2154	2154	4	0	100.00	99.81	0.19
220	2048	2048	0	0	100.00	100.00	0.00
221	2427	2427	6	0	100.00	99.75	0.25
222	2483	2482	4	1	99.96	99.84	0.20
223	2605	2604	2	1	99.96	99.92	0.12
228	2053	2051	1	2	99.90	99.95	0.15
230	2256	2256	0	0	100.00	100.00	0.00
231	1571	1571	0	0	100.00	100.00	0.00
232	1780	1780	2	0	100.00	99.89	0.11
233	3079	3076	1	3	99.90	99.97	0.13

Rec. No.	<i>TB</i>	<i>TP</i>	<i>FP</i>	<i>FN</i>	<i>Se(%)</i>	<i>P+(%)</i>	<i>DER(%)</i>
234	2753	2753	0	0	100.00	100.00	0.00
Total	109494	109205	130	289	99.74	99.88	0.38

Table 3.2: Comparison with state-of-the-art methods

Sr. No.	Reference	<i>Se(%)</i>	<i>P+(%)</i>	<i>DER(%)</i>
1	Pan et al. (1985) [7]	99.76	99.56	0.68
2	Zidelmal et al. (2012) [22]	99.64	99.82	0.54
3	Pandit et al. (2017) [39]	99.65	99.66	0.69
4	Zalabarría et al. (2020)[36]	99.54	99.6	0.86
5	The proposed method	99.74	99.88	0.38

3.4 Conclusion

In this chapter, a single channel QRS complex detection using Wavelet denoising, median filtering, and AMT, was proposed. The proposed method has shown high robustness and can adapt to abrupt changes in morphology in the ECG signals. The method is successfully evaluated on a standard database of 48 records taken from both male and female participants, age between 23 to 89 which is a highly diverse age range. The proposed method has shown significant improvement in terms of automatic detection of heartbeats and its performance is compatible with the requirements for detection applications.

Algorithm 2 The proposed algorithm for AMT.

- 1: Read X samples of the input ECG signal
- 2: Preprocessing using DWT and denoising filters (median filters, moving average filter), as in Section 3.2.1
- 3: Process full record with amplitude 320 ms minimum peak-to-peak interval
- 4: Compute the local peaks and store the locations and amplitudes in vectors \mathbf{L} and \mathbf{P} , respectively, with each having a length of N , as in Section 3.2.2
- 5: Compute T , by using (3.1)
- 6: Initialize S , by using (3.2)
- 7: Initialize M , by using (3.3)
- 8: Initialize R , by using (3.4)
- 9: Initialize V_{sl} and V_{nl} , as in Section 3.2.2
- 10: $B_w = 0$
- 11: $B_z = 0$
- 12: Let $i = 1$
- 13: **while** $i < N$
- 14: **if** $P(i) \geq S$
- 15: Store $P(i)$ in \mathbf{G}
- 16: Store $L(i)$ in \mathbf{H}
- 17: Update V_{sl} , by using (3.5)
- 18: **elseif** $P(i) < S$ and $P(i) \geq M$
- 19: Compute $B(i)$, by using (3.6)
- 20: Compute B_w , by using (3.7)
- 21: **if** $B(i) \leq B_w$
- 22: Store $P(i)$ in \mathbf{G}
- 23: Store $L(i)$ in \mathbf{H}
- 24: Update V_{sl} , by using (3.8)
- 25: **else**
- 26: Update V_{nl} , by using (3.9)
- 27: **End**
- 28: **elseif** $P(i) < M$ and $P(i) \geq R$
- 29: Compute $B(i)$, by using (3.6)
- 30: Compute B_z , by using (3.10)
- 31: **if** $B(i) \leq B_z$,
- 32: Store $P(i)$ in \mathbf{G}
- 33: Store $L(i)$ in \mathbf{H}
- 34: Update V_{sl} , by using (3.8)
- 35: **else**
- 36: Update V_{nl} , by using (3.9)
- 37: **End**
- 38: **End**
- 39: Update and store beat rate in vector \mathbf{B} , by using (3.6)
- 40: Update M , by using(3.11)
- 41: Update R , by using (3.12)
- 42: $i = i + 1$
- 43: **End**

```

44: Compute peak-to-peak intervals and store in vector  $\mathbf{K}$ , by using (3.13)
45: Compute  $F$ , by using (3.14)
46: Let  $n = 1$ .
47:  $A = \text{Length of vector } \mathbf{K}$ 
48: while  $n < A$ 
49:   if  $K(n) \geq F$ 
      • Find peaks in that interval with minimum peak-to-peak interval  $0.8 * F$  and
        minimum amplitude threshold of  $0.2 * M$  and store the peaks  $\mathbf{Z}_t$ 
50:   End
51:  $n = n + 1$ 
52: End
53: Return  $\mathbf{Z}_t$ 

```

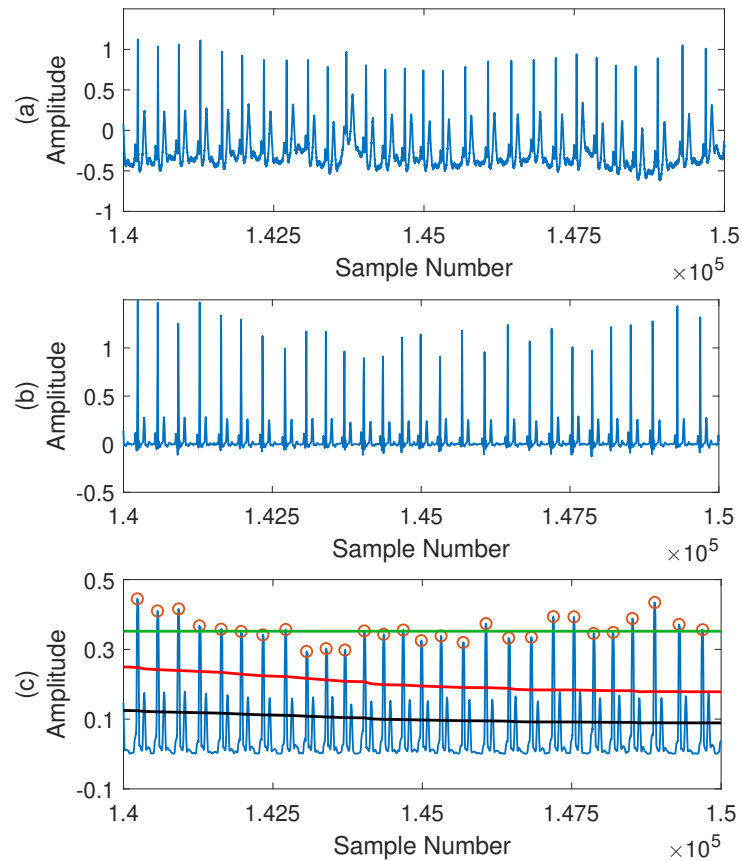


Figure 3.5: A section of record 108 from MIT-BIH arrhythmia database with y-axis in mV (388-416s). (a) Raw ECG signal, (b) Signal obtained after median filtering, (c) Peaks detected on the envelope of the signal. The green, red and black lines represent the non-adaptive threshold S , the upper adaptive threshold M and lower adaptive threshold R , respectively.

Chapter 4

QRS Detection Using Adaptive Multilevel Thresholding, Segmentation and Statistical False Peak Elimination

4.1 Introduction

Normally, Q, R, and S are three deflections where Q and S have negative amplitudes, and R has a positive amplitude in the ECG signal. The main problem encountered by earlier algorithms in the detection of R-peaks and ectopic beats is the presence of electromyogram (EMG) signal and irregular intervals between peaks. While EMG signals have similar amplitudes to that of the R-peaks, they also show peaks at positions where there should be R-peaks and so it is difficult to recognize the R-peaks when ECG and EMG signals are mixed. One way of removing the peaks due to the EMG signal is by using false peak elimination and segmentation. While adaptive multilevel thresholding is effective in separating the noise peaks from the QRS peaks because of the changing amplitude of the threshold, it is not so efficient in adapting to the change in peak-to-peak intervals and EMG signal interference. This chapter aims to present a new technique for detecting QRS using adaptive multilevel thresholding (AMT), segmentation, and statistical false peak elimination. The method is tested by simulation using the MIT-BIH arrhythmia database [51] and [52].

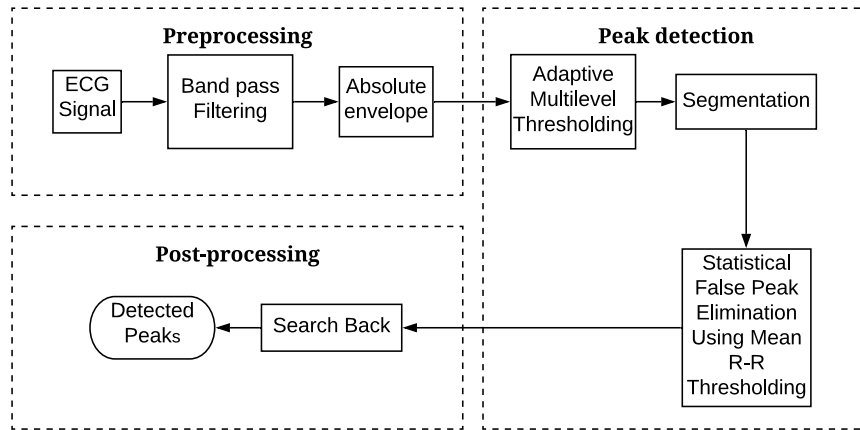


Figure 4.1: Block diagram of the proposed method.

4.2 The Proposed Method

Figure 4.1 shows the block diagram of the proposed method. Like the earlier methods, this technique also has three stages which are a preprocessing stage, a peak detection stage, and a post-processing stage. The preprocessing stage is put in place to extract the maximum information of the ECG signal while minimizing both the high and low-frequency noises. The peak detection stage here is divided into two substages and detects peaks twice to enhance the processing of the ECG signal. The first substage uses multilevel adaptive thresholding with two distinct adaptive thresholds to detect the R-peaks and the premature ventricular contractions (PVCs). The second substage uses segmentation and statistical false peak elimination to analyze the already detected peaks to remove false positives. Finally, the post-processing stage will process the entire record and search for missed peaks with low amplitudes.

4.2.1 Preprocessing

Here, instead of using several steps, a bandpass filter is used with passband edge frequencies of 5 Hz and 35 Hz, respectively. As mentioned in Chapter 1, the main information of the ECG remains within this frequency band, and therefore for the algorithm to work, the selected frequency band is enough to detect the peaks properly. The peak amplitudes of the P and T waves are also reduced if any frequency lower than 5 Hz is eliminated. Using the bandpass filter, however, does not reduce the amplitude of the EMG signal and loses some information of the R-peaks as a certain percentage of their information remains above 35 Hz. Figure 4.2 shows the signal processed by the bandpass filter. Figure 4.2(a) shows an ECG signal that has a baseline wander while

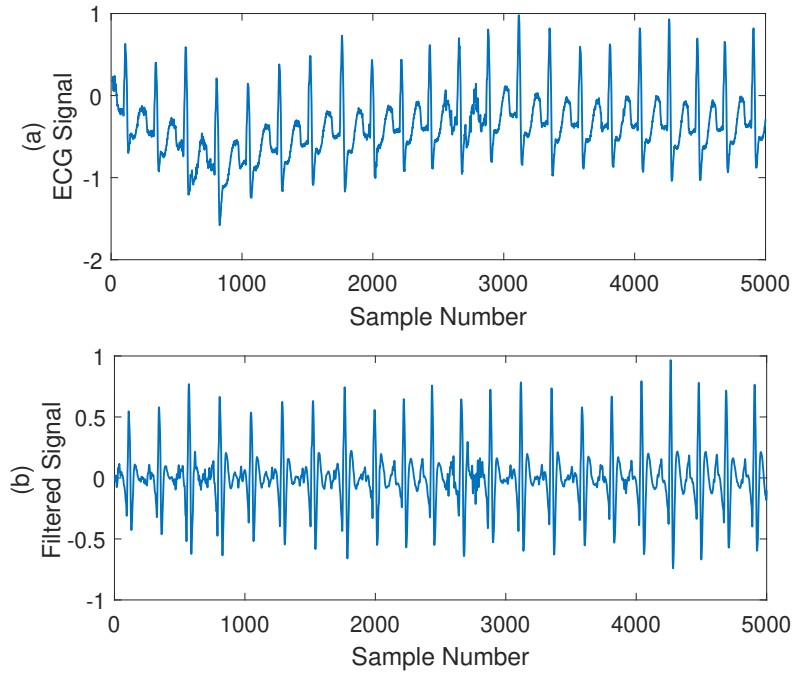


Figure 4.2: Baseline wander removal. (a) ECG signal with baseline wander, (b) Band-pass filtered signal after removing baseline wander.

Fig. 4.2(b) shows that the baseline has been corrected with slight fluctuations that do not hamper the detection. The bandpass filter can remove the powerline interference as it remains well outside the frequency range of the desired passband frequency range and that is illustrated in Fig. 4.3 shows this effect.

Once the signal is filtered by using bandpass filter, the signal is normalized using the formula,

$$X_{norm} = \frac{X}{X_{maximum}}, \quad (4.1)$$

where, X is the signal processed by the bandpass filter and $X_{maximum}$ is the maximum amplitude of the whole signal. The absolute value of the signal is then taken and smoothed using a window of 50 ms. This does not affect the R-peaks or ectopic beats much and reduces the P and T wave amplitudes further as these waves occur approximately 100 ms before and after the QRS complex, respectively, and have lower slopes. The smoothing process employs a moving average filter. Figure 4.4 shows the envelope taken after the smoothing process. Figure 4.4(a) shows the raw ECG signal of record 104 from the MIT-BIH arrhythmia database while Fig. 4.4(b) shows the bandpass filtered signal and Fig. 4.4(c) shows the smoothed or enveloped signal.

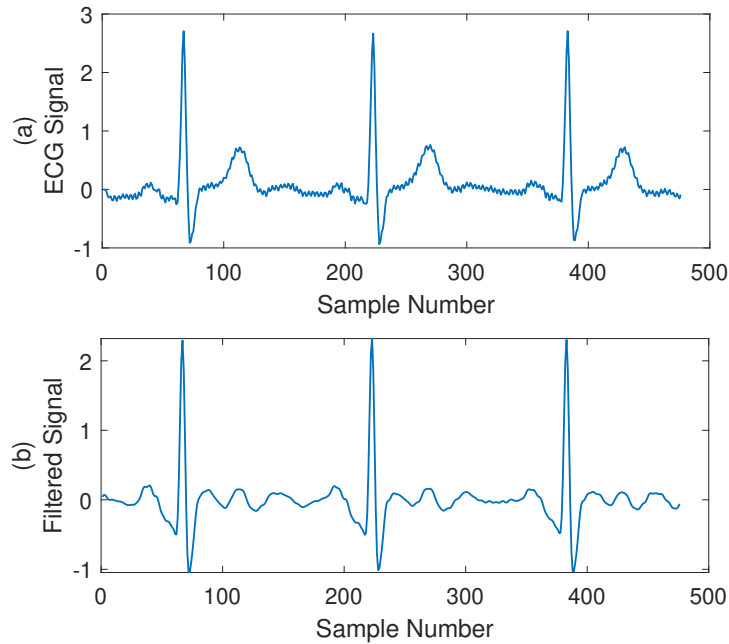


Figure 4.3: Powerline interference removal. (a) ECG signal with powerline interference, (b) Powerline interference removed after bandpass filtering.

4.2.2 Peak detection using adaptive multilevel thresholding and statistical peak-to-peak interval analysis

After the preprocessing stage is complete, the peak detection stage starts with initializing the minimum interval between peaks to 280 ms. The reason for this is that the algorithm in Chapter 2 faced some problems while taking 320 ms to be the minimum peak-to-peak interval. Many true positives were eliminated in certain records containing ectopic beats. Even though it is a beat rate over 200 beats/min which is regarded as ventricular flutter [55], some records show that the beat rate can go above 200 beats/min which creates many false negatives for those records if approximately 190 beats/min or 3.15 beats/s is set as the beat rate threshold. Therefore, to keep false negatives as minimum as possible, a beat rate of approximately 215 beats/min or 3.60 beats/s is allowed in this algorithm. Any extra false positives resulting from this change are eliminated later using statistical false peak elimination.

Adaptive Multilevel Thresholding

Once all the local peaks are found, their amplitudes and locations are stored in vector \mathbf{P} and \mathbf{L} , respectively. The vectors \mathbf{P} and \mathbf{L} are given by, $\mathbf{P} = [P(1), P(2), P(3), \dots, P(N)]$

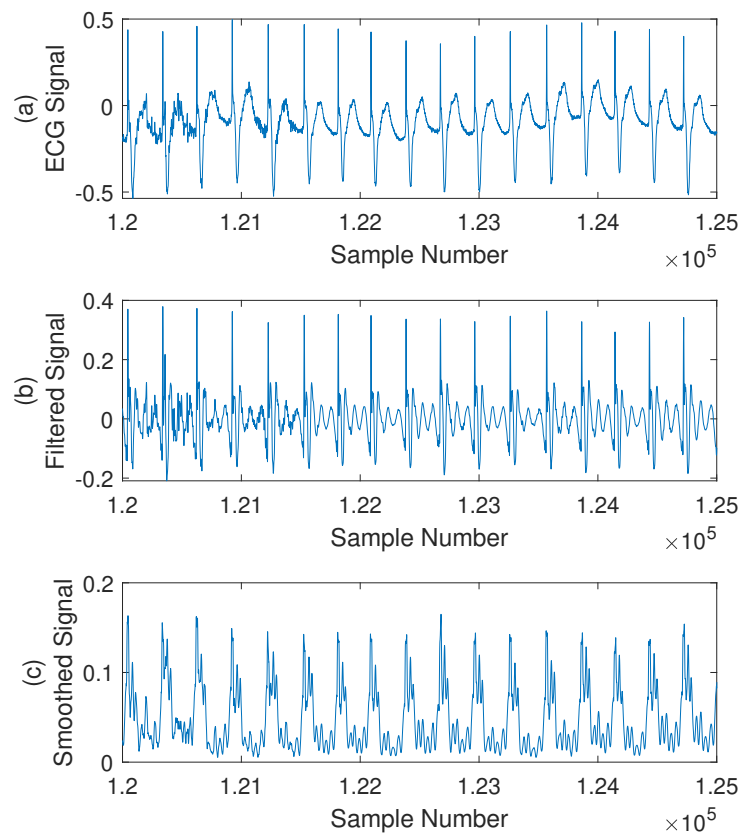


Figure 4.4: Outputs obtained from record 104 with y-axis in mV (333-346s). (a) The raw ECG Signal, (b) The bandpass filtered signal, (c) The preprocessed signal.

and $\mathbf{L} = [L(1), L(2), L(3), \dots, L(N)]$, where N is the total number of local peaks. The average value of the amplitudes of all these peaks in \mathbf{P} , denoted by T , is calculated using,

$$T = \frac{\sum_{n=1}^N P(n)}{N}, \quad (4.2)$$

where n is the position of the peak in vector \mathbf{P} .

Two distinct levels of the signal, signal value (V_{sl}), and noise value (V_{nl}) are initialized to be 0. These values are used to update the thresholds with each selected true peak or discarded noise peak. Two initial thresholds are also set to process the obtained peaks, which are M , and R as,

$$M = T, \quad (4.3)$$

$$R = 0.6T. \quad (4.4)$$

Here, R is regarded as the lower adaptive amplitude threshold below which all peaks are regarded as noise peaks and hence eliminated. The value M is the upper adaptive threshold and any peak amplitude in vector \mathbf{P} that exceeds this value will be regarded as a pseudo-true peak. The signal value for the true peaks detected using this threshold is updated using,

$$V_{sl} = 0.1a + 0.9V_{sl}, \quad (4.5)$$

where a is the amplitude of the pseudo-true peak. The algorithm also stores the detected pseudo-true peaks in vectors \mathbf{G} and \mathbf{H} as pseudo-true peak amplitudes and pseudo-true peak locations, respectively. Here, the vectors, \mathbf{G} and \mathbf{H} are given by, $\mathbf{G} = [G(1), G(2), G(3), \dots, G(Q)]$ and $\mathbf{H} = [H(1), H(2), H(3), \dots, H(Q)]$, where Q is the total number of pseudo-true peaks. However, if a peak is found to be less than the threshold M and above threshold R , the beat rate is calculated in contrast to the detected peak preceding it. This is calculated by using,

$$B(i) = \frac{60f_s}{H(i+1) - H(i)}, \quad (4.6)$$

where i is the instantaneous position of the beat rate in vector \mathbf{B} . If it is found that the instantaneous beat rate, $B(i)$, is less than the beat rate threshold, B_w , then the peak is regarded as the pseudo-true peak. Here, B_w is given by,

$$B_w = \frac{1.75 \sum_{i=3}^{Q-1} B(i)}{Q-4}. \quad (4.7)$$

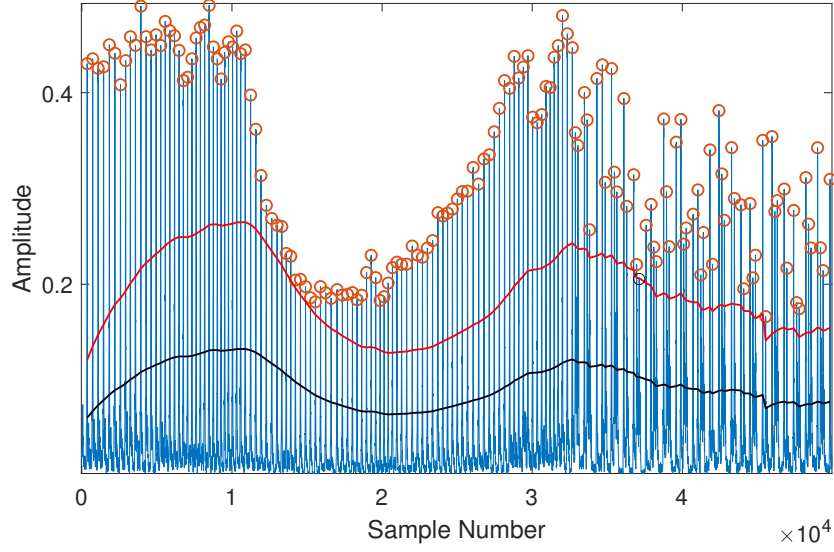


Figure 4.5: Multilevel adaptive thresholding.

However, if this is not the case and $B(i)$ is greater than B_w , then the peak is regarded as a noise peak and discarded and the noise value is updated by,

$$V_{nl} = 0.2a + 0.8V_{nl}. \quad (4.8)$$

Any peaks falling below threshold R are also regarded as noise peaks and will be discarded and the value of V_{nl} will again be updated using (4.8). After classifying the peak as a true peak or a noise peak, the threshold M is updated using,

$$M = 0.6V_{nl} + 0.6(V_{sl} - V_{nl}), \quad (4.9)$$

and the threshold R is updated as,

$$R = 0.5M. \quad (4.10)$$

Once the thresholds are calculated again the entire process will be repeated for the next peak and the thresholds will be updated. Figure 4.5 shows how the two adaptive thresholds change with the rise and fall in the amplitudes of the signal peaks. The process is similar to the one in Chapter 3, however, the weights for M and the beat rate have been altered to make the thresholds more adaptive and higher than the previous ones. This results in more accurate detection and lowers false negatives.

Segmentation

Once all the pseudo-true peaks are found using adaptive multilevel thresholding the ECG signal is divided into several segments, each having no more than 50000 samples. The process is similar to the one used in Chapter 2, however, the number of segments used here is exactly half the number of segments used in Chapter 2 as the number of samples per segment is twice the number used in Chapter 2. Vectors \mathbf{G} and \mathbf{H} are also divided into the same number of segments according to where their values should be placed in the ECG signal. The value 50000 was selected to enhance the accuracy of the algorithm with respect to peak-to-peak intervals without losing too many samples. It is important to note that unlike the method in Chapter 2, there will be no peak overlapping as the peaks are selected using the whole ECG record rather than by using a segment. Thus, the number of steps decreases along with the number of computations used.

Statistical false peak elimination

Once the segmentation is complete the pseudo-true peaks are analyzed by calculating the intervals between adjacent peaks to that of the mean peak-to-peak interval of the whole segment. Let the vector $\mathbf{Y} = [Y(1), Y(2), Y(3), \dots, Y(C)]$ represents all the locations of pseudo-true peaks in the segment and let the vector $\mathbf{Z} = [Z(1), Z(2), Z(3), \dots, Z(C)]$ represents all the pseudo-true peak values in the segment and let C be the number of values in vectors \mathbf{Y} and \mathbf{Z} . The mean proportional value of all the weights in vector \mathbf{Z} , called F is also calculated using,

$$F = 0.8 \frac{\sum_{e=1}^C Z(e)}{C}, \quad (4.11)$$

where e is the position of the values in each vector. Next, let a third vector $\mathbf{D}_{fp} = [D_{fp}(1), D_{fp}(2), D_{fp}(3) \dots, D_{fp}(C-1)]$ be formed that contains all the peak-to-peak intervals calculated from vector \mathbf{Y} , such that,

$$D_{fp}(e) = Y(e+1) - Y(e). \quad (4.12)$$

Now, the average proportional value, W , of the mean of the values in vector \mathbf{D}_{fp} is formulated using the equation,

$$W = k \frac{\sum_{e=1}^{C-1} D_{fp}(e)}{C-1}, \quad (4.13)$$

where k is equal to 0.75 and 0.5 for low and high morphological changes, respectively, and e is the position of the peak values and peak locations in \mathbf{Z} and \mathbf{Y} , respectively.

Now, if a peak value in vector \mathbf{Z} with an instantaneous position $v+1$, is smaller than F , we compare the corresponding value in vector \mathbf{D}_{fp} with the position v , with W . If it is found that $D_{fp}(v)$ is less than W , then $D_{fp}(v+1)$ is also compared to W . If $D_{fp}(v+1)$ is also found to be smaller, then the algorithm guarantees that there is a false peak at position $D_{fp}(v)$. The location corresponding to $D_{fp}(v)$ that is $Y(v+1)$ will be removed along with $Z(v+1)$ and a new interval between the peaks will be established using the formula,

$$D_{fp}(v) = D_{fp}(v) + D_{fp}(v+1). \quad (4.14)$$

This goes on for each pseudo-true peak in the segment that has a lesser value than F . This reduces the number of computations as well because unlike the algorithm in Chapter 2, we do not need to process all the pseudo-true peaks. The algorithm only processes the peaks which are low in amplitude and very close to each other. Thus, the number of the falsely detected peaks is reduced further without eliminating any ectopic beats. The step is repeated for each segment and, finally, all the peak locations from all the segments together are obtained and stored in vector \mathbf{A} , where $\mathbf{A} = [A(1), A(2), A(3), \dots, A(J)]$ and their corresponding amplitudes in vector \mathbf{E} , where $\mathbf{E} = [E(1), E(2), E(3), \dots, E(J)]$. Here, J is the total number of true peak obtained after statistical false peak elimination. Figure 4.6 shows the effect of using this stage on a segment of record 104. The record contains interference from EMG on some parts and a section of 50000 samples are shown which contains high amounts of noise. Figure 4.6(a) displays a peak falsely detected due to high-frequency noise while Fig. 4.6(b) shows the false peak that was eliminated.

4.2.3 Post-processing

The aim of this stage is to search for low amplitude missed peaks by taking the peak-to-peak intervals for the detected peaks of the whole ECG record into consideration.

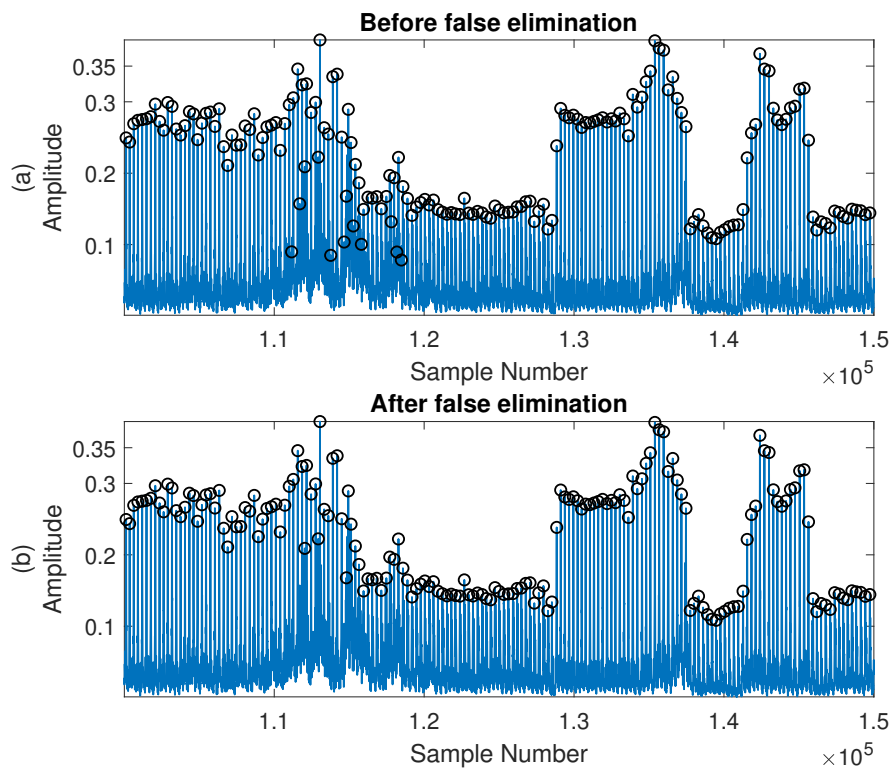


Figure 4.6: False peak elimination in record 104 with y-axis in mV (277-347s) of MIT-BIH arrhythmia database. (a) False peaks detected after preprocessing, (b) False peaks removed after using statistical false peak elimination.

Once all the true peak locations are found and stored in vector \mathbf{A} , the peak-to-peak intervals are calculated and stored in vector \mathbf{D}_{sb} , using,

$$D_{sb}(u) = A(u+1) - A(u), \quad (4.15)$$

where u is the instantaneous position of the peaks in \mathbf{A} and \mathbf{E} .

Here, $\mathbf{D}_{sb} = [D_{sb}(1), D_{sb}(2), D_{sb}(3), \dots, D_{sb}(J-1)]$. Here, the total length of \mathbf{D}_{sb} is $J-1$ as two peak locations from vector \mathbf{A} is needed to calculate the interval between them. Hence, an x-axis threshold for the maximum peak-to-peak interval allowed between adjacent peaks will be calculated using,

$$S = \frac{1.75 \sum_{a=1}^{J-1} D_{sb}(a)}{J-1}. \quad (4.16)$$

If it is found that the interval between any two adjacent peaks exceeds the value of S then the search back will be triggered and it will search for peaks within that interval between the corresponding peaks by lowering the amplitude threshold to 25% of the initial value of M and peak-to-peak interval to 50% the value of S . Any peaks obtained through this method is regarded as a low amplitude missed peak and is added to the vectors \mathbf{A} and \mathbf{E} at their corresponding positions as true peaks. Figure 4.7 shows the detection of a missed peak in record 109 which was detected using the search back procedure. The process is repeated for the entire record to ensure maximum accuracy in detection.

4.3 Experiment and Results

The MIT-BIH arrhythmia database with 48 records each with a duration of half an hour is used in this experiment. Only channel 1 was used for the experiment and a total of 142.5 seconds of data from record 207 is excluded which contains ventricular flutter. The evaluation of the proposed method uses the same figure of merits from Chapter 2 and 3, which are sensitivity (Se), positive predictivity ($P+$), and detection error rate (DER). These quantities are repeated here for clarity and they are represented by,

$$Se = \frac{TP}{TP + FN}, \quad (4.17)$$

$$P+ = \frac{TP}{TP + FP}, \quad (4.18)$$

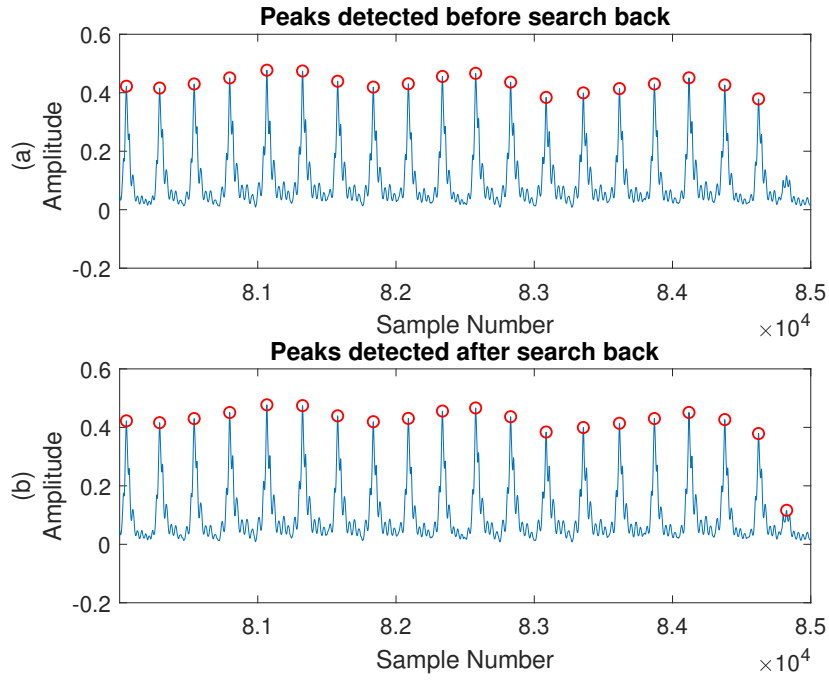


Figure 4.7: False peak elimination in record 109 with y-axis in mV (222-236s) of MIT-BIH arrhythmia database. (a) False peak eliminated signal, (b) Missed peak detected on the preprocessed signal after using search back.

$$DER = \frac{FP + FN}{TB}, \quad (4.19)$$

where TP is the number of true positives, FP is the number of false negatives, FN is the number of false positives and TB is the total number of beats annotated in the record. The algorithm of the entire approach is summarized in Algorithm 3. Table 4.1 represents the results of running 48 records from the MIT-BIH arrhythmia database. The results obtained are better than the previous methods included in the literature as well as the algorithms evaluated in Chapter 2 and 3. The proposed method shows a high sensitivity of 99.85%, a positive predictivity of 99.91%, and a detection error rate of only 0.25%. The proposed method is further compared to five other state-of-the-art methods and shows a better detection rate than all of them. This is represented in Table 4.2.

Table 4.1: Results from the MIT-BIH arrhythmia database

Rec. No.	TB	TP	FP	FN	$Se(\%)$	$P+(\%)$	$DER(\%)$
100	2273	2273	0	0	100.00%	100.00%	0.00%
101	1865	1865	3	0	100.00%	99.84%	0.16%
102	2187	2187	0	0	100.00%	100.00%	0.00%

Rec. No.	<i>TB</i>	<i>TP</i>	<i>FP</i>	<i>FN</i>	<i>Se(%)</i>	<i>P+(%)</i>	<i>DER(%)</i>
103	2084	2083	0	1	99.95%	100.00%	0.05%
104	2229	2229	7	0	100.00%	99.69%	0.31%
105	2572	2572	21	0	100.00%	99.19%	0.82%
106	2027	2028	3	2	100.05%	100.00%	0.25%
107	2137	2131	0	6	99.72%	100.00%	0.28%
108	1763	1762	3	1	99.94%	99.83%	0.23%
109	2532	2532	0	0	100.00%	100.00%	0.00%
111	2124	2124	0	0	100.00%	100.00%	0.00%
112	2539	2539	2	0	100.00%	99.92%	0.08%
113	1795	1795	0	0	100.00%	100.00%	0.00%
114	1879	1876	2	3	99.84%	99.89%	0.27%
115	1953	1953	0	0	100.00%	100.00%	0.00%
116	2412	2395	0	17	99.30%	100.00%	0.70%
117	1535	1535	1	0	100.00%	99.93%	0.07%
118	2278	2278	0	0	100.00%	100.00%	0.00%
119	1987	1987	2	0	100.00%	99.90%	0.10%
121	1863	1865	2	1	100.11%	100.00%	0.16%
122	2476	2476	0	0	100.00%	100.00%	0.00%
123	1518	1516	0	2	99.87%	100.00%	0.13%
124	1619	1617	1	2	99.88%	99.94%	0.19%
200	2601	2599	0	2	99.92%	100.00%	0.08%
201	1963	1950	0	13	99.34%	100.00%	0.66%
202	2136	2131	1	5	99.77%	99.95%	0.28%
203	2980	2944	13	36	98.79%	99.56%	1.64%
205	2656	2647	0	9	99.66%	100.00%	0.34%
207	1860	1854	5	6	99.68%	99.73%	0.59%
208	2955	2943	0	12	99.59%	100.00%	0.41%
209	3005	3002	0	3	99.90%	100.00%	0.10%
210	2650	2611	8	39	98.53%	99.69%	1.77%
212	2748	2748	0	0	100.00%	100.00%	0.00%
213	3251	3249	0	2	99.94%	100.00%	0.06%
214	2262	2262	1	0	100.00%	99.96%	0.04%
215	3363	3361	1	2	99.94%	99.97%	0.09%
217	2208	2206	0	2	99.91%	100.00%	0.09%
219	2154	2154	1	0	100.00%	99.95%	0.05%
220	2048	2048	0	0	100.00%	100.00%	0.00%

Rec. No.	<i>TB</i>	<i>TP</i>	<i>FP</i>	<i>FN</i>	<i>Se(%)</i>	<i>P+(%)</i>	<i>DER(%)</i>
221	2427	2425	0	2	99.92%	100.00%	0.08%
222	2483	2483	24	0	100.00%	99.04%	0.97%
223	2605	2605	0	0	100.00%	100.00%	0.00%
228	2053	2053	0	0	100.00%	100.00%	0.00%
230	2256	2256	0	0	100.00%	100.00%	0.00%
231	1571	1571	0	0	100.00%	100.00%	0.00%
232	1780	1780	2	0	100.00%	99.89%	0.11%
233	3079	3078	0	1	99.97%	100.00%	0.03%
234	2753	2753	0	0	100.00%	100.00%	0.00%
Total	109494	109331	103	169	99.85%	99.91%	0.25%

Table 4.2: Comparison with state-of-the-art methods

Sr. No.	Reference	Year	<i>P+(%)</i>	<i>Se(%)</i>	<i>DER(%)</i>
1	Pan et al. [7]	1985	99.56	99.76	0.68
2	Pandit et al. [39]	2017	99.66	99.65	0.69
3	Sahrma et al. [25]	2019	99.83	99.89	0.29
4	Zalabarría et al. [36]	2020	99.6	99.54	0.86
5	Bouny et al. [24]	2020	99.87	99.84	0.3
6	Proposed Method	2020	99.91	99.85	0.25

Figure 4.8 shows the overall detection of peaks in a segment record 113. As seen here the P and T waves do not impose any threat to the algorithm.

Table 4.3 shows the comparison of the method proposed in this chapter with those proposed in Chapters 2, and 3, respectively. The development of algorithms in Chapters 2, and 3, have led to the development of the algorithm in this chapter. In the proposed algorithm in Chapter 2, the processes of segmentation and statistical false peak elimination were developed, however, the amplitude threshold was non-adaptive which gave rise to several false positives and negatives. In the proposed algorithm in Chapter 3, adaptive amplitude and beat rate thresholding for several levels were introduced. For the algorithm developed in this chapter, both of these stages were combined to provide the maximum accuracy for detection as shown in the table. The table also shows the decrease in the number of false positives and negatives while positive predictivity, sensitivity, and detection error rate have increased significantly.

Algorithm 3 The proposed algorithm.

- 1: Read X samples of the input ECG signal
 - 2: Preprocessing using bandpass filter and moving average filtering, as in Section 4.2.1
 - 3: Normalize the obtained signal, by using (4.1)
 - 4: Process full record with amplitude 280 ms minimum peak-to-peak interval
 - 5: Compute the local peaks and store the locations and amplitudes in vectors \mathbf{L} and \mathbf{P} , respectively, with each having a length of N , as in Section 4.2.2
 - 6: Compute T , by using (4.2)
 - 7: Initialize M , by using (4.3)
 - 8: Initialize R , by using (4.4)
 - 9: Initialize V_{sl} and V_{nl} , by M and R , respectively.
 - 10: $B_w = 0$
 - 11: Let $i = 1$
 - 12: **while** $i < N$
 - 13: **if** $P(i) \geq M$,
 - 14: Store $P(i)$ in \mathbf{G}
 - 15: Store $L(i)$ in \mathbf{H}
 - 16: Update V_{sl} , by using (4.5)
 - 17: **elseif** $P(i) < M$ and $P(i) \geq R$
 - 18: Compute $B(i)$, by using (4.6)
 - 19: Compute B_w , by using (4.7)
 - 20: **if** $B(i) \leq B_w$
 - 21: Store $P(i)$ in \mathbf{G}
 - 22: Store $L(i)$ in \mathbf{H}
 - 23: Update V_{sl} , by using (4.5)
 - 24: **else**
 - 25: Update V_{nl} , by using (4.8)
 - 26: **End**
 - 27: **End**
 - 28: Update and store beat rate in vector \mathbf{B} , by using (4.6)
 - 29: Update M , by using (4.9)
 - 30: Update R , by using (4.10)
 - 31: $i = i + 1$.
 - 32: **End**
 - 33: Divide G and H into C number of segments of j samples each
 - 34: Let $i = 1$
 - 35: **while** $i < C$
 - 36: Input segment number i of H
 - 37: Compute F , by using (4.11)
 - 38: Compute D_{fp} , by using (4.12)
 - 39: Compute W , by using (4.13)
-

```

40:   Eliminate false peaks to obtain  $\mathbf{y}$ , by using (4.14)
41:    $\mathbf{Y} = [\mathbf{Y} \quad \mathbf{y}]$ 
42:    $i = i + 1$ 
43: End
44: Process  $\mathbf{Y}$  and compute peak-to-peak intervals and store in vector  $\mathbf{D}_{sb}$ , by using
    (4.15)
45: Compute  $S$ , by using (4.16)
46: Let  $n = 1$ 
47:  $Q =$  Length of vector  $\mathbf{D}_{sb}$ 
48: while  $n < Q$ 
49:   if  $\mathbf{D}_{sb} \geq S$ 
      • Find peaks in that interval with minimum peak-to-peak interval  $0.5*S$  and
        minimum amplitude threshold of  $0.25*M$  and store the peaks  $\mathbf{Z}$ 
50:   End
51:  $n = n + 1$ 
52: End
53:  $\mathbf{Z}_t = [\mathbf{Y} \quad \mathbf{Z}]$ 
54: Return  $\mathbf{Z}_t$ 

```

Table 4.3: Comparison with methods in the developing stages

Sr. No.	Methods	FN	FP	$P+(\%)$	$Se(\%)$	$DER(\%)$
1	Chapter 2	200	136	99.88	99.82	0.31
2	Chapter 3	289	130	99.88	99.74	0.38
3	Chapter 4	169	103	99.91	99.85	0.25

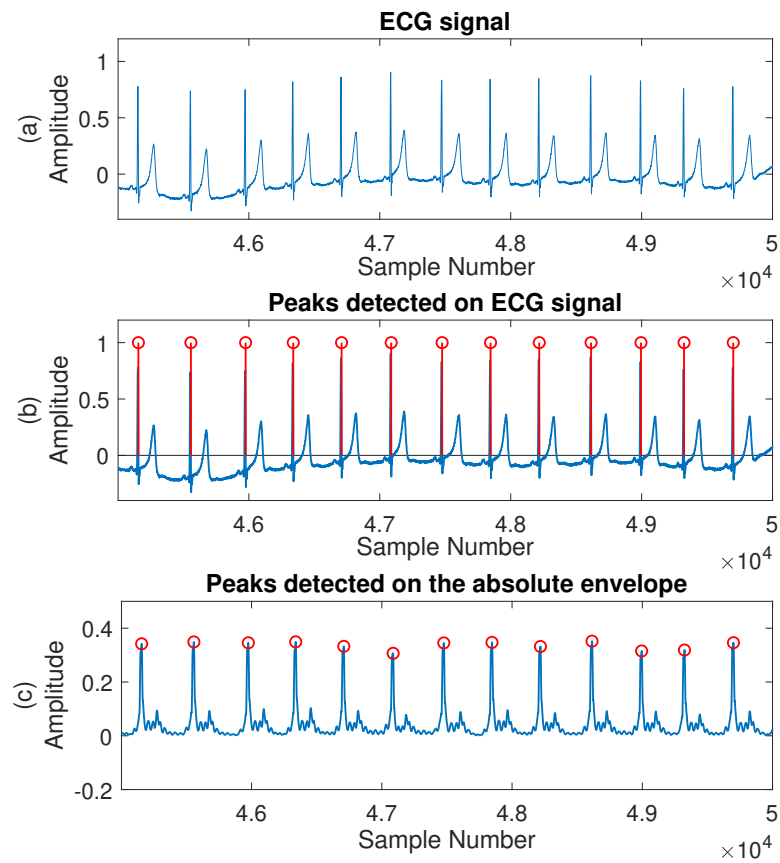


Figure 4.8: Peak detection performed in record 113 with y-axis in mV (125-139s). (a) The raw ECG signal, (b) Peaks detected on the ECG signal, (c) Peaks detected on the preprocessed signal.

4.4 Conclusion

In this chapter, the combination of adaptive multilevel thresholding, segmentation, and statistical false peak elimination, was proposed. The proposed method is highly robust and can adapt to abrupt changes in morphology of the ECG signals. The method has been successfully evaluated on a standard database of 48 records taken from both male and female participants, age between 23 to 89 which is a highly diverse age range. The proposed method has been tested on the MIT-BIH database and shows better results than any other method mentioned in the thesis. This method has also shown significant improvements in terms of automatic detection of heartbeats and its performance is compatible with the requirements for detection applications.

Chapter 5

Conclusions and Future Work

5.1 Conclusions

In this thesis, new approaches for peak detection in ECG signals have been presented. The approaches have taken into consideration mean R-R intervals, adaptive amplitude thresholds and beat rates, to correctly identify the QRS complexes and the ectopic beats. The algorithms show high accuracy in detecting peaks and displays much robustness in adapting to the changes in morphology in the ECG signals. The algorithms have been tested on the MIT-BIH database [51] using MATLAB. The Fantasia [52] and parts of the European ST-T database [54] were also used for the algorithm in Chapter 2. The annotations of these databases are available online and were used to check the peak locations for the proposed methods. The MIT-BIH arrhythmia database has an immense number of variations in morphology in the ECG signal and presents challenging ECG records from a variety of age groups. The records contain noise variations as well as variations in ectopic beats and most of the records are from patients with major abnormalities in their heart rhythm. The proposed method, in Chapter 1, has achieved a sensitivity (Se) of 99.85%, a positive predictivity (P+) of 99.91%, and a detection error rate (DER) of 0.25% overall for the MIT-BIH arrhythmia database. The novel method of QRS detection using multidimensional thresholds and statistical false peak elimination was also tested on the Fantasia database and has achieved a sensitivity, a positive predictivity, and a detection error rate of 99.92%, 99.90%, and 0.18% respectively. This makes the proposed methods adaptive to sudden changes in the ECG signal, high amounts of noise, and swift fluctuations encountered due to a fast-changing heart rhythm.

In this research, three algorithms to detect QRS complexes have been developed. The proposed methods have been compared to several state-of-the-art techniques in the

field and shows better accuracy in detection than most of those methods. The method in Chapter 2 uses automatic segmentation which breaks down the ECG signals into smaller segments for fast and accurate comparison of the peak-to-peak intervals with the average peak-to-peak interval of a particular segment. Breaking down a signal into smaller segments also makes the algorithm adaptable to the morphological changes in signal. Statistical false peak elimination has also been used that aids in eliminating interference from high-frequency noise and EMG signals. The method in Chapter 3 emphasizes on adaptive multilevel thresholds that can be used to detect peaks more accurately than simple non-adaptive thresholds. The final method in Chapter 4 combined both the methods from Chapter 2 and 3 to provide an algorithm that is efficient in both detecting true peaks and eliminating false peaks while decreasing the number of segments used in Chapter 2. The algorithm has been devised to eliminate the need for memory-intensive filtering and transformations. This has resulted in better detection accuracy.

5.2 Future Work

In our work, we have studied QRS complexes and ectopic beats. However, the notion of ventricular or atrial flutter or fibrillation detection was not considered in this work and is a key area of research in this field. Flutters are deadly vibrations of heart muscles that almost always lead to death or permanent damage to the heart, the brain, and other organs of the body. Therefore, the next goal of this work is to create an algorithm that can detect ventricular and atrial flutter or fibrillation. The main idea is taking into consideration the peak-to-peak intervals of ventricular or atrial flutter which exceeds the range of 200 beats/min for the normal rhythm of heart beats. Ventricular flutter also resembles sinusoidal waves and this feature can be further studied to detect these types of abnormalities. Furthermore, future research may also consist of studies on ectopic beats. By taking into account the position and amplitudes of the P and T waves and by measuring their slopes, distinguishing between rhythmic QRS complexes and ectopic beats like premature ventricular and atrial contractions and premature junctional complexes, can be conducted..

BIBLIOGRAPHY

- [1] Rangayyan, R. M. (2015). Biomedical signal analysis (Vol. 33). John Wiley & Sons.
- [2] Boyett, M. R. (2009). 'And the beat goes on' The cardiac conduction system: the wiring system of the heart. *Experimental physiology*, 94(10), 1035-1049.
- [3] Whitaker, R. H. (2010). Anatomy of the heart. *Medicine*, 38(7), 333-335.
- [4] Davies, A., & Scott, A. (2013). Arrhythmias. In *Starting to Read ECGs* (pp. 79–107). Springer London. https://doi.org/10.1007/978-1-4471-4962-0_6
- [5] Aladin, A. I., Whelton, S. P., Al-Mallah, M. H., Blaha, M. J., Keteyian, S. J., Juraschek, S. P., ... & Michos, E. D. (2014). Relation of resting heart rate to risk for all-cause mortality by gender after considering exercise capacity (the Henry Ford exercise testing project). *The American journal of cardiology*, 114(11), 1701–1706.
- [6] Drake, J. D., & Callaghan, J. P. (2006). Elimination of electrocardiogram contamination from electromyogram signals: An evaluation of currently used removal techniques. *Journal of electromyography and kinesiology*, 16(2), 175-187.
- [7] Pan, J., & Tompkins, W. J. (1985). A real-time QRS detection algorithm. *IEEE transactions on biomedical engineering*, (3), 230-236.
- [8] Hamilton, P. S., & Tompkins, W. J. (1986). Quantitative investigation of QRS detection rules using the MIT/BIH arrhythmia database. *IEEE transactions on biomedical engineering*, (12), 1157-1165.
- [9] Lu, X., Pan, M., & Yu, Y. (2018). QRS detection based on improved adaptive threshold. *Journal of healthcare engineering*, 2018.

- [10] Arteaga-Falconi, J., Al Osman, H., & El Saddik, A. (2015, May). R-peak detection algorithm based on differentiation. In 2015 IEEE 9th International Symposium on Intelligent Signal Processing (WISP) Proceedings (pp. 1-4). IEEE.
- [11] Deboleena Sadhu Khan and Madhuchhanda Mitra, "R-Peak detection algorithm for ECG using double difference and RR interval processing, *Procedia Technology* 4 (2012) 873-877.
- [12] Yun-Chi Yeh and Wen-June Wang, "QRS Complexes detection for ECG signal: The Difference Operation Method," *Computer methods and Programs in Biomedicine* 91 (2008) 245-254, www.intl.elsevierhealth.com/journals/cmpb.
- [13] Sharma, T., & Sharma, K. K. (2017). QRS complex detection in ECG signals using locally adaptive weighted total variation denoising. *Computers in biology and medicine*, 87, 187–199.
- [14] Kohler, B. U., Hennig, C., & Orglmeister, R. (2002). The principles of software QRS detection. *IEEE Engineering in Medicine and biology Magazine*, 21(1), 42-57.
- [15] Kadambe, S., Murray, R., & Boudreaux-Bartels, G. F. (1999). Wavelet transform-based QRS complex detector. *IEEE Transactions on biomedical Engineering*, 46(7), 838-848.
- [16] Pal, S., & Mitra, M. (2010). Detection of ECG characteristic points using multiresolution wavelet analysis based selective coefficient method. *Measurement*, 43(2), 255-261.
- [17] Singh, O., & Sunkaria, R. K. (2011). A robust R-peak detection algorithm using wavelet packets. *Int. J. Comput. Appl*, 36, 37-43.
- [18] Haddadi, R., Abdelmounim, E., El Hanine, M., & Belaguid, A. (2014, April). Discrete wavelet transform based algorithm for recognition of QRS complexes. In 2014 International Conference on Multimedia Computing and Systems (ICMCS) (pp. 375-379). IEEE.
- [19] Gokhale, P. S. (2012). ECG Signal De-noising using Discrete Wavelet Transform for removal of 50Hz PLI noise. *International Journal of Emerging Technology and Advanced Engineering*, 2(5), 81-85.
- [20] Dinh, H. A. N., Kumar, D. K., Pah, N. D., & Burton, P. (2001). Wavelets for QRS detection. *Australasian Physics & Engineering Sciences in Medicine*, 24(4), 207

- [21] Martínez, J. P., Almeida, R., Olmos, S., Rocha, A. P., & Laguna, P. (2004). A wavelet-based ECG delineator: evaluation on standard databases. *IEEE Transactions on biomedical engineering*, 51(4), 570-581.
- [22] Zidelmal, Z., Amirou, A., Adnane, M., & Belouchrani, A. (2012). QRS detection based on wavelet coefficients. *Computer methods and programs in biomedicine*, 107(3), 490-496.
- [23] Madan, R., Singh, S. K., & Jain, N. (2009). Signal filtering using discrete wavelet transform. *International journal of recent trends in engineering*, 2(3), 96.
- [24] El Bouny, L., Khalil, M., & Adib, A. (2020). A Wavelet Denoising and Teager Energy Operator-Based Method for Automatic QRS Complex Detection in ECG Signal. *Circuits, Systems, and Signal Processing*, 1–37.
- [25] Sharma, A., Patidar, S., Upadhyay, A., & Acharya, U. R. (2019). Accurate tunable-Q wavelet transform based method for QRS complex detection. *Computers & Electrical Engineering*, 75, 101–111.
- [26] Benitez, D., Gaydecki, P. A., Zaidi, A., & Fitzpatrick, A. P. (2001). The use of the Hilbert transform in ECG signal analysis. *Computers in biology and medicine*, 31(5), 399-406.
- [27] Sahoo, S., Biswal, P., Das, T., & Sabut, S. (2016). De-noising of ECG signal and QRS detection using Hilbert transform and adaptive thresholding. *Procedia Technology*, 25, 68-75.
- [28] Farahabadi, A., Farahabadi, E., Rabbani, H., & Mahjoub, M. P. (2012, January). Detection of QRS complex in electrocardiogram signal based on a combination of hilbert transform, wavelet transform and adaptive thresholding. In *Proceedings of 2012 IEEE-EMBS International Conference on Biomedical and Health Informatics* (pp. 170-173). IEEE.
- [29] D'Aloia, M., Longo, A., & Rizzi, M. (2019). Noisy ECG signal analysis for automatic peak detection. *Information*, 10(2), 35.
- [30] Pal, S., & Mitra, M. (2012). Empirical mode decomposition based ECG enhancement and QRS detection. *Computers in biology and medicine*, 42(1), 83-92.
- [31] Slimane, Z. E. H., & Naït-Ali, A. (2010). QRS complex detection using empirical mode decomposition. *Digital Signal Processing*, 20(4), 1221-1228.

- [32] Tang, J., Zou, Q., Tang, Y., Liu, B., & Zhang, X. K. (2007, July). Hilbert-Huang transform for ECG de-noising. In 2007 1st international conference on bioinformatics and biomedical engineering (pp. 664-667). IEEE.
- [33] Peng, Z. K., Peter, W. T., & Chu, F. L. (2005). A comparison study of improved Hilbert–Huang transform and wavelet transform: application to fault diagnosis for rolling bearing. *Mechanical systems and signal processing*, 19(5), 974-988.
- [34] Satija, U., Ramkumar, B., & Manikandan, M. S. (2018). A new automated signal quality-aware ECG beat classification method for unsupervised ECG diagnosis environments. *IEEE Sensors Journal*, 19(1), 277–286.
- [35] Jain, S., Ahirwal, M. K., Kumar, A., Bajaj, V., & Singh, G. K. (2017). QRS detection using adaptive filters: A comparative study. *ISA transactions*, 66, 362–375.
- [36] Zalabarria, U., Irigoyen, E., Martinez, R., & Lowe, A. (2020). Online robust R-peaks detection in noisy electrocardiograms using a novel iterative smart processing algorithm. *Applied Mathematics and Computation*, 369, 124839.
- [37] Hao, W., Chen, Y., & Xin, Y. (2011, September). ECG baseline wander correction by mean-median filter and discrete wavelet transform. In 2011 Annual International Conference of the IEEE Engineering in Medicine and Biology Society (pp. 2712–2715). IEEE.
- [38] Christov, I. I. (2004). Real time electrocardiogram QRS detection using combined adaptive threshold. *Biomedical engineering online*, 3(1), 28.
- [39] Pandit, D., Zhang, L., Liu, C., Chattopadhyay, S., Aslam, N., & Lim, C. P. (2017). A lightweight QRS detector for single lead ECG signals using a max-min difference algorithm. *Computer methods and programs in biomedicine*, 144, 61–75.
- [40] Mathews, S. M., Kambhamettu, C., & Barner, K. E. (2018). A novel application of deep learning for single-lead ECG classification. *Computers in biology and medicine*, 99, 53–62.
- [41] Xiang, Y., Lin, Z., & Meng, J. (2018). Automatic QRS complex detection using two-level convolutional neural network. *Biomedical engineering online*, 17(1), 13.

- [42] Sannino, G., & De Pietro, G. (2018). A deep learning approach for ECG-based heartbeat classification for arrhythmia detection. *Future Generation Computer Systems*, 86, 446–455.
- [43] Yıldırım, Ö., Pławiak, P., Tan, R. S., & Acharya, U. R. (2018). Arrhythmia detection using deep convolutional neural network with long duration ECG signals. *Computers in biology and medicine*, 102, 411–420.
- [44] Pławiak, P., & Acharya, U. R. (2020). Novel deep genetic ensemble of classifiers for arrhythmia detection using ECG signals. *Neural Computing and Applications*, 32(15), 11137–11161.
- [45] Tang, X., Hu, Q., & Tang, W. (2018). A real-time QRS detection system with PR/RT interval and ST segment measurements for wearable ECG sensors using parallel delta modulators. *IEEE transactions on biomedical circuits and systems*, 12(4), 751–761.
- [46] Hou, Z., Dong, Y., Xiang, J., Li, X., & Yang, B. (2018). A real-time QRS detection method based on phase portraits and box-scoring calculation. *IEEE Sensors Journal*, 18(9), 3694–3702.
- [47] Lin, C. (2011). P and T wave detection in electrocardiogram (ECG) signals. Signal & Communications Group, University of Toulouse.
- [48] Zhang, Z., Yu, Q., Zhang, Q., Ning, N., & Li, J. (2020). A Kalman filtering based adaptive threshold algorithm for QRS complex detection. *Biomedical Signal Processing and Control*, 58, 101827.
- [49] “CDC - Chronic Disease - Heart Disease and Stroke Prevention - At A Glance,” 2011.
- [50] Rezaeian, I., & Rueda, L. (2014). CMT: A constrained multi-level thresholding approach for ChIP-Seq data analysis. *Plos one*, 9(4), e93873.
- [51] Moody, G. B., & Mark, R. G. (2001). The impact of the MIT-BIH arrhythmia database. *IEEE Engineering in Medicine and Biology Magazine*, 20(3), 45-50.
- [52] Iyengar, N., Peng, C. K., Morin, R., Goldberger, A. L., & Lipsitz, L. A. (1996). Age-related alterations in the fractal scaling of cardiac interbeat interval dynamics. *American Journal of Physiology-Regulatory, Integrative and Comparative Physiology*, 271(4), R1078–R1084.

- [53] Goldberger, A. L., Amaral, L. A., Glass, L., Hausdorff, J. M., Ivanov, P. C., Mark, R. G., ... & Stanley, H. E. (2000). PhysioBank, PhysioToolkit, and PhysioNet: components of a new research resource for complex physiologic signals. *circulation*, 101(23), e215–e220.
- [54] Taddei, A., Distanti, G., Emdin, M., Pisani, P., Moody, G. B., Zeelenberg, C., & Marchesi, C. (1992). The European ST–T database: standard for evaluating systems for the analysis of ST–T changes in ambulatory electrocardiography. *European heart journal*, 13(9), 1164–1172.
- [55] Koster, R. W., & Wellens, H. J. (1976). Quinidine-induced ventricular flutter and fibrillation without digitalis therapy. *The American journal of cardiology*, 38(4), 519–523.
- [56] Aladin, A. I., Whelton, S. P., Al-Mallah, M. H., Blaha, M. J., Keteyian, S. J., Juraschek, S. P., ... & Michos, E. D. (2014). Relation of resting heart rate to risk for all-cause mortality by gender after considering exercise capacity (the Henry Ford exercise testing project). *The American journal of cardiology*, 114(11), 1701–1706.

VITA AUCTORIS

Sudipta Modak was born in 1991, in Rajbari, Bangladesh. He graduated from Maple Leaf International School in Dhaka, Bangladesh in 2010. He continued to pursue his education at BRAC University, Dhaka, Bangladesh. He graduated from BRAC University with a B.Sc. in Electrical and Electronics Engineering, with a major in electronics in 2015. Sudipta is currently pursuing a M.A.Sc. degree at the University of Windsor and hopes to graduate in Fall 2020.